SI Appendix

Supplementary Figures

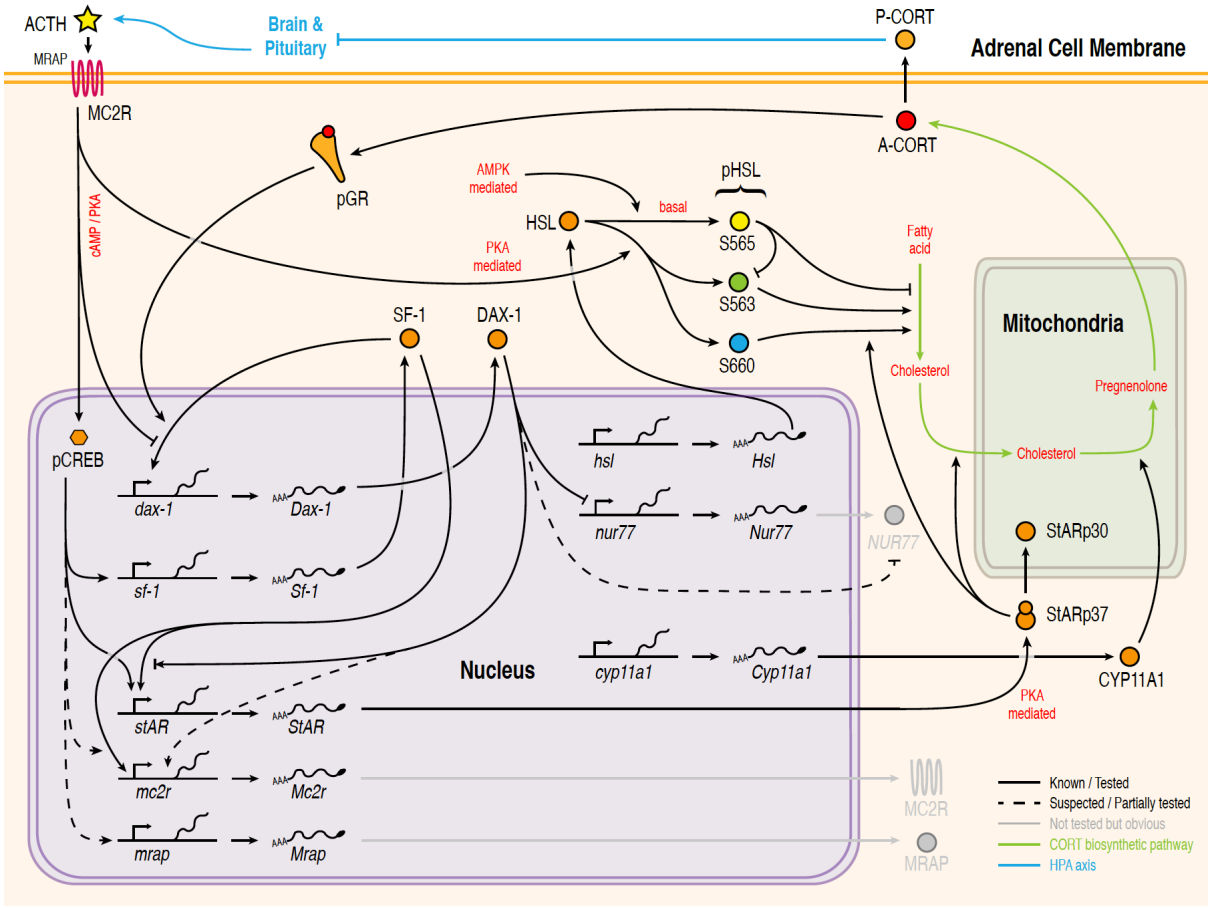

Fig. S1. The steroidogenic regulatory network (SRN). The synthesis of glucocorticoids in adrenocortical cells is governed at multiple levels by both genomic and non-genomic components. In addition to the high degree of cross-talk between these components, an intra-adrenal feedback loop mediated by A-CORT/GR may underlie adrenal responsiveness and maintain appropriate levels of glucocorticoids.

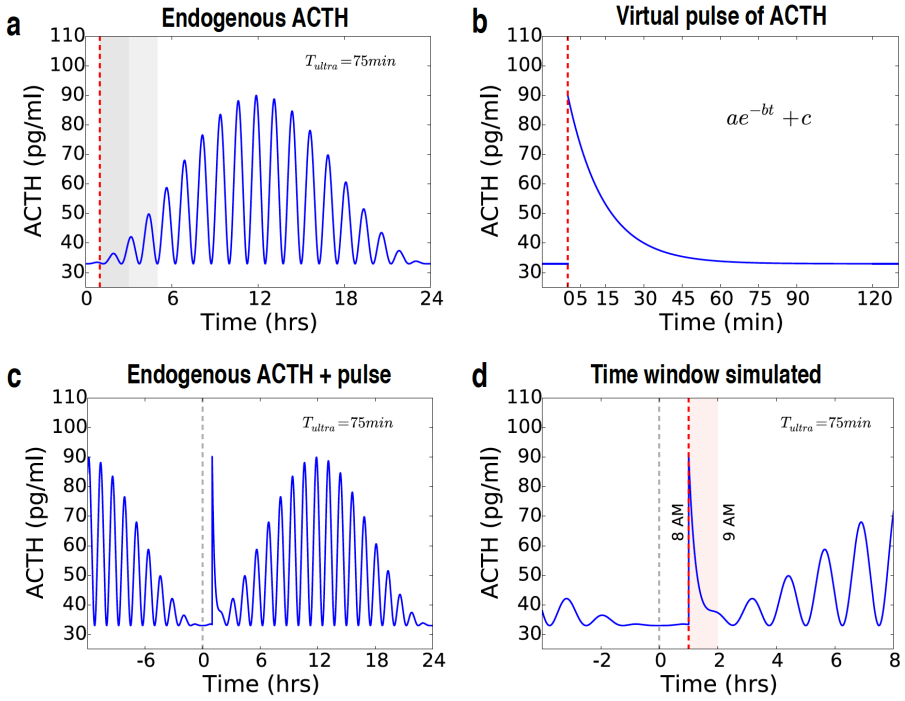

Fig. S2. Virtual (*in silico*) computer simulations of ACTH endogenous oscillations and perturbations. (a) The model was driven by oscillating levels of ACTH that represented endogenous fluctuations. **(b)** A simple function representing a "virtual" pulse of ACTH. **(c)** The pulse was of a size comparable to the maximum endogenous levels in normal physiological conditions. **(d)** The "virtual" pulse was given near the nadir of the circadian ACTH rhythm, at approximately the same time corresponding to the *in vivo* experiments (between 8 and 9 AM).

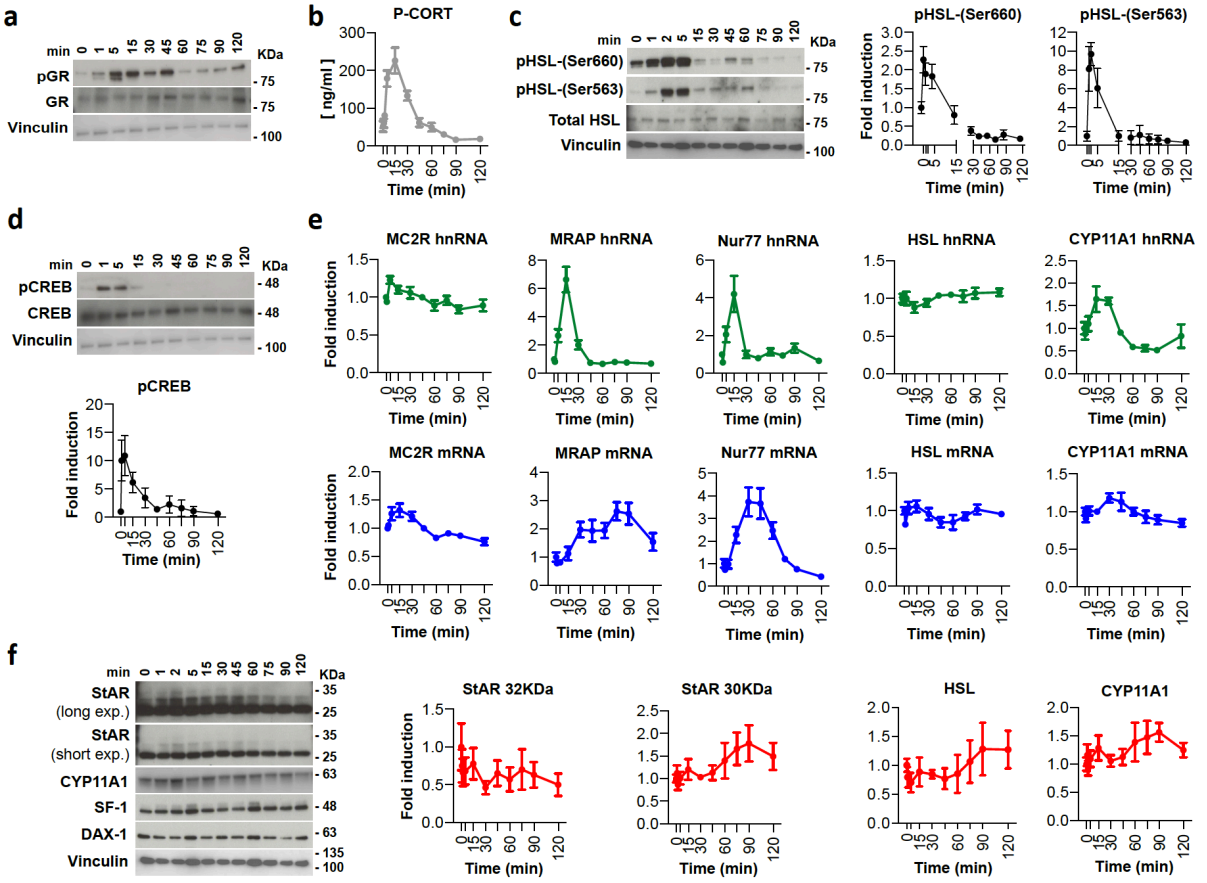

Fig. S3. A short pulse of ACTH dynamically activates the SRN and CORT biosynthesis. (a) Representative Western immunoblotting of the effect of a pulse of ACTH on intra-adrenal phospho-GR (quantification is shown in Fig. 2c in the main text). **(b)** A pulse of ACTH dynamically affects plasma CORT (P-CORT). **(c)** Representative Western immunoblotting and quantification of the dynamic effect of a pulse of ACTH on phosphorylation of HSL (pHSL-(Ser660) and pHSL-(Ser563)). **(d)** Representative Western immunoblotting and quantification of the dynamic effect of a pulse of ACTH on phosphorylation of CREB in Ser133. **(e)** A pulse of ACTH dynamically affects plasma CORT steroidogenic genes hnRNA and mRNA. **(f)** Representative Western immunoblotting and quantification of the dynamic effect of a pulse of ACTH on steroidogenic protein expression (quantification of StARp37, SF-1 and DAX-1 proteins is shown in Fig. 2 in the main text). For Western immunoblotting data, optical density was normalised to Vinculin; for RTqPCR, data were normalised to GAPDH mRNA levels; Western immunoblotting and RTqPCR data are expressed as fold induction of time 0 (n=4-7/time point). Details of asymptotic significances are reported in Table S2.

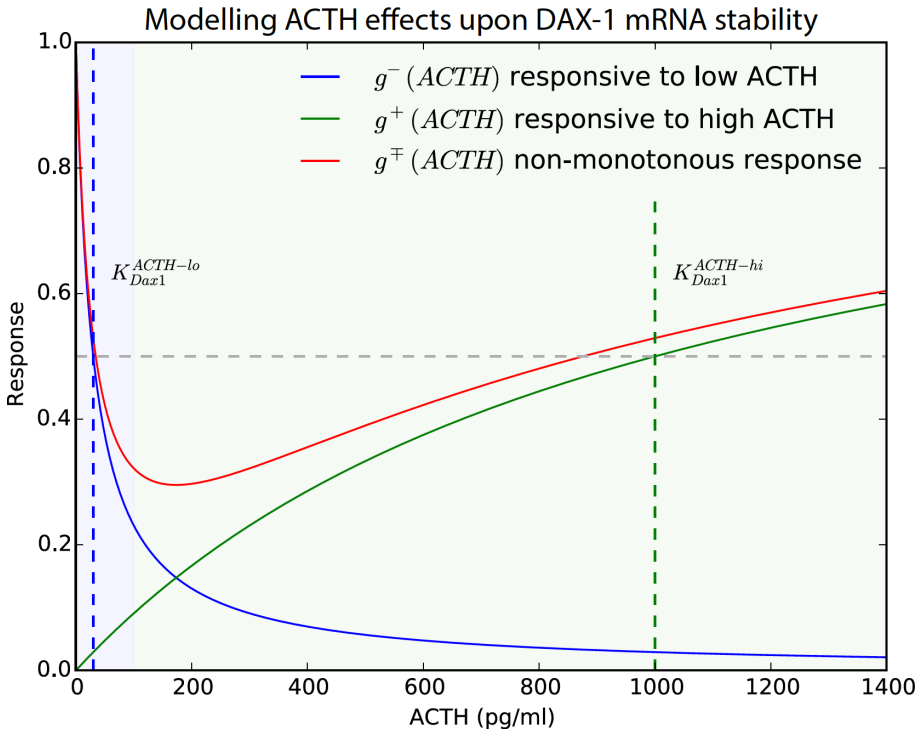

Fig. S4. Modelling ACTH dose-dependent effects on DAX-1 mRNA stability. While an increasing function g^{+} is supported by previous experiments performed at high doses of ACTH, only a decreasing function g^{-} fits our *in vivo* experiments at low doses of ACTH. We hypothesise a non-monotonous –decreasing, then increasing– response mechanism that successfully reproduces our data at both low and high doses of ACTH.

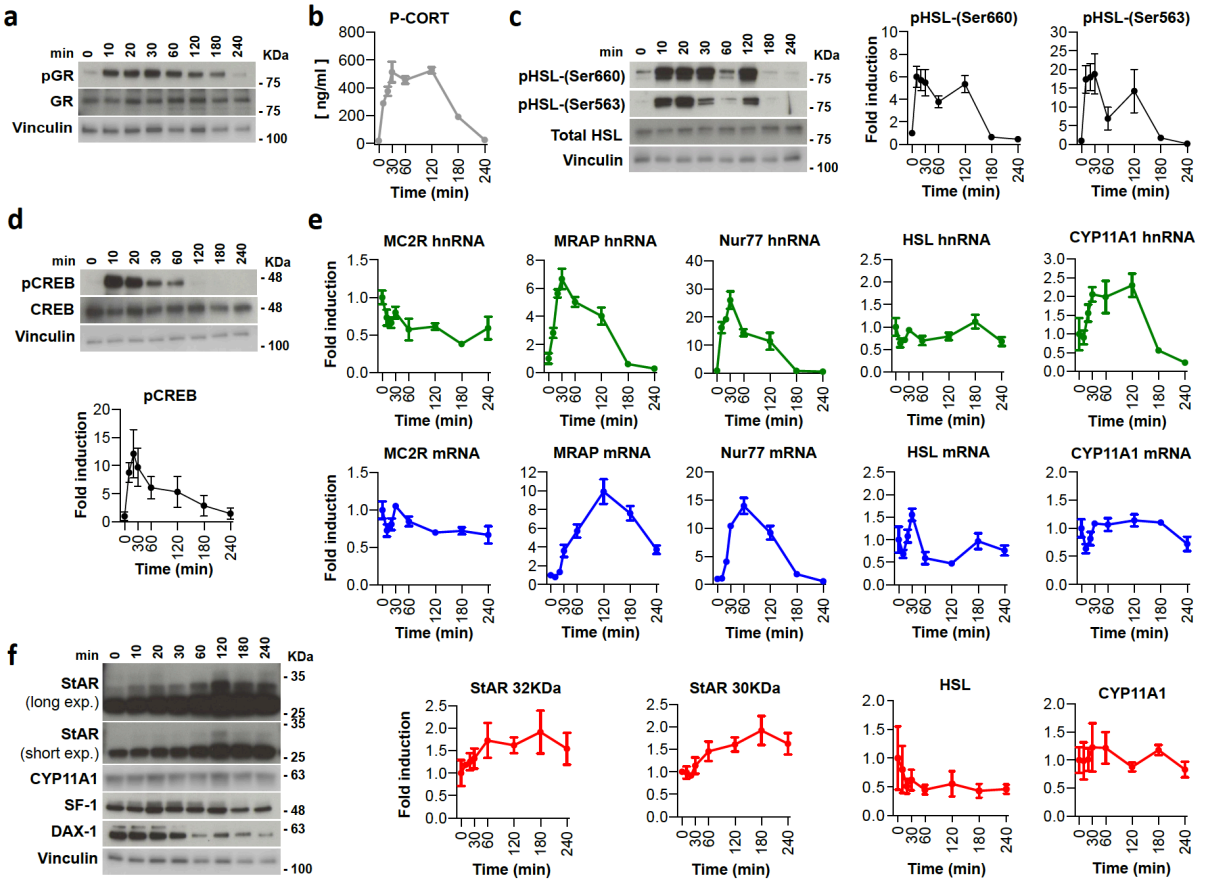

Fig. S5. Dynamic synthesis of adrenal glucocorticoids and activity of the SRN following a high dose of ACTH. (a) Representative Western immunoblotting of the effect of a high dose of ACTH on intra-adrenal phospho-GR (quantification is shown in Fig. 3c in the main text). **(b)** A high dose of ACTH dynamically affects plasma CORT (P-CORT). **(c)** Representative Western immunoblotting and quantification of the dynamic effect of a high dose of ACTH on phosphorylation of HSL (pHSL-(Ser660) and pHSL-(Ser563)). **(d)** Representative Western immunoblotting and quantification of the dynamic effect of a high dose of ACTH on phosphorylation of CREB in Ser133. **(e)** A high dose of ACTH dynamically affects plasma CORT steroidogenic genes hnRNA and mRNA. **(f)** Representative Western immunoblotting and quantification of the dynamic effect of a high dose of ACTH on steroidogenic protein expression (quantification of StARp37, SF-1 and DAX-1 proteins is shown in Fig. 3 in the main text). For Western immunoblotting data, optical density was normalised to Vinculin; for RTqPCR, data were normalised to GAPDH mRNA levels; Western immunoblotting and RTqPCR data are expressed as fold induction of time 0 (n=4/time point). Details of asymptotic significances are reported in Table S2.

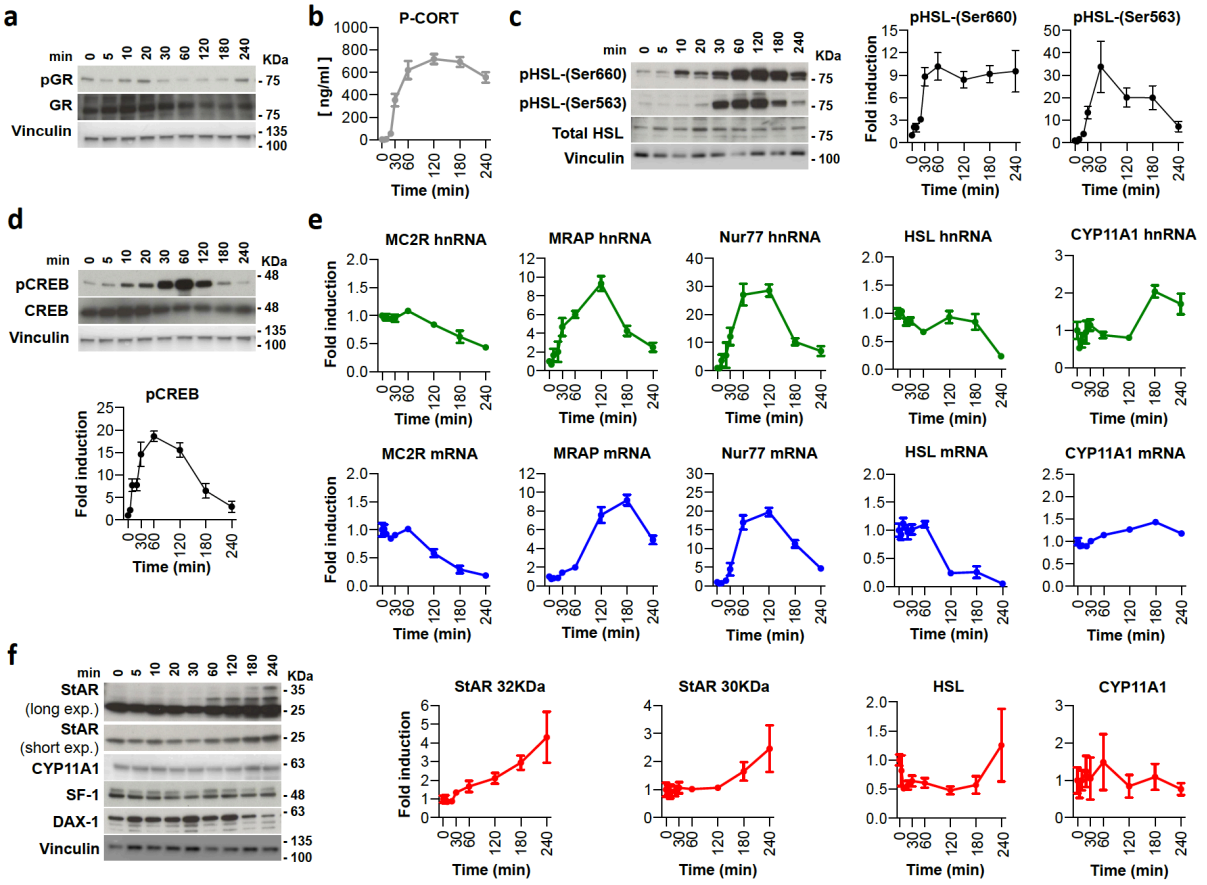

Fig. S6. Dynamic synthesis of adrenal glucocorticoids and activity of the SRN following administration of LPS. (a) Representative Western immunoblotting of the effect of LPS on intra-adrenal phospho-GR (quantification is shown in Fig. 4c in the main text). **(b)** Administration of LPS dynamically affects plasma CORT (P-CORT). **(c)** Representative Western immunoblotting and quantification of the dynamic effect of LPS on phosphorylation of HSL (pHSL-(Ser660) and pHSL-(Ser563)). **(d)** Representative Western immunoblotting and quantification of the dynamic effect of LPS on phosphorylation of CREB in Ser133. **(e)** Administration of LPS dynamically affects plasma CORT steroidogenic genes hnRNA and mRNA. **(f)** Representative Western immunoblotting and quantification of the dynamic effect of LPS on steroidogenic protein expression (quantification of StARp37, SF-1 and DAX-1 proteins is shown in Fig. 4 in the main text). For Western immunoblotting data, optical density was normalised to Vinculin; for RTqPCR, data were normalised to GAPDH mRNA levels; Western immunoblotting and RTqPCR data are expressed as fold induction of time 0 (n=4-12/time point). Details of asymptotic significances are reported in Table S2.

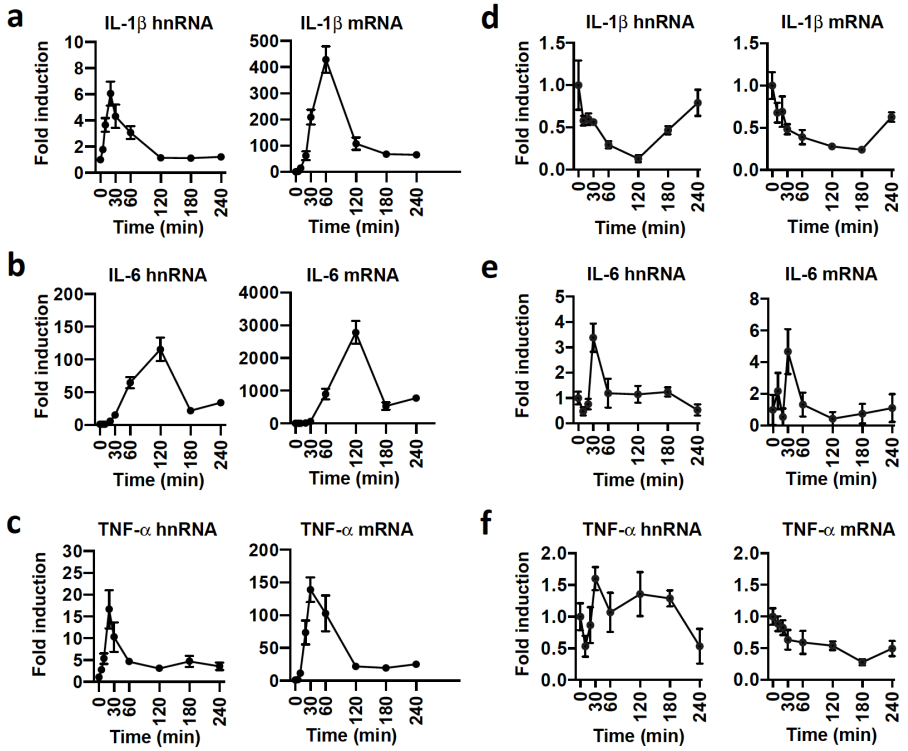

Fig. S7. Effect of LPS vs direct administration of a high dose of ACTH on intra-adrenal cytokines gene expression. The effect of LPS and high s.c. ACTH was evaluated by measuring the hnRNA and mRNA dynamics by RTqPCR (n=4-5/time point). Data are expressed as fold induction of time 0. LPS administration dynamically increased **(a)** IL-1β hnRNA (P<0.0001) and mRNA (P<0.0001), **(b)** IL-6 hnRNA (P<0.0001) and mRNA (P<0.0001), and **(c)** TNF-α hnRNA (P=0.006) and mRNA (P<0.0001). In contrast, administration of a high dose of ACTH significant decreased **(d)** IL-1β hnRNA (P=0.005) and mRNA (P=0.003), whereas only a small but significant increase was observed in **(e)** IL-6 hnRNA (P=0.03) but not on mRNA (P=0.171), and a trend toward significant increase and a significant decrease was observed in **(f)** TNF-α hnRNA (P=0.067) and mRNA (P=0.02), respectively.

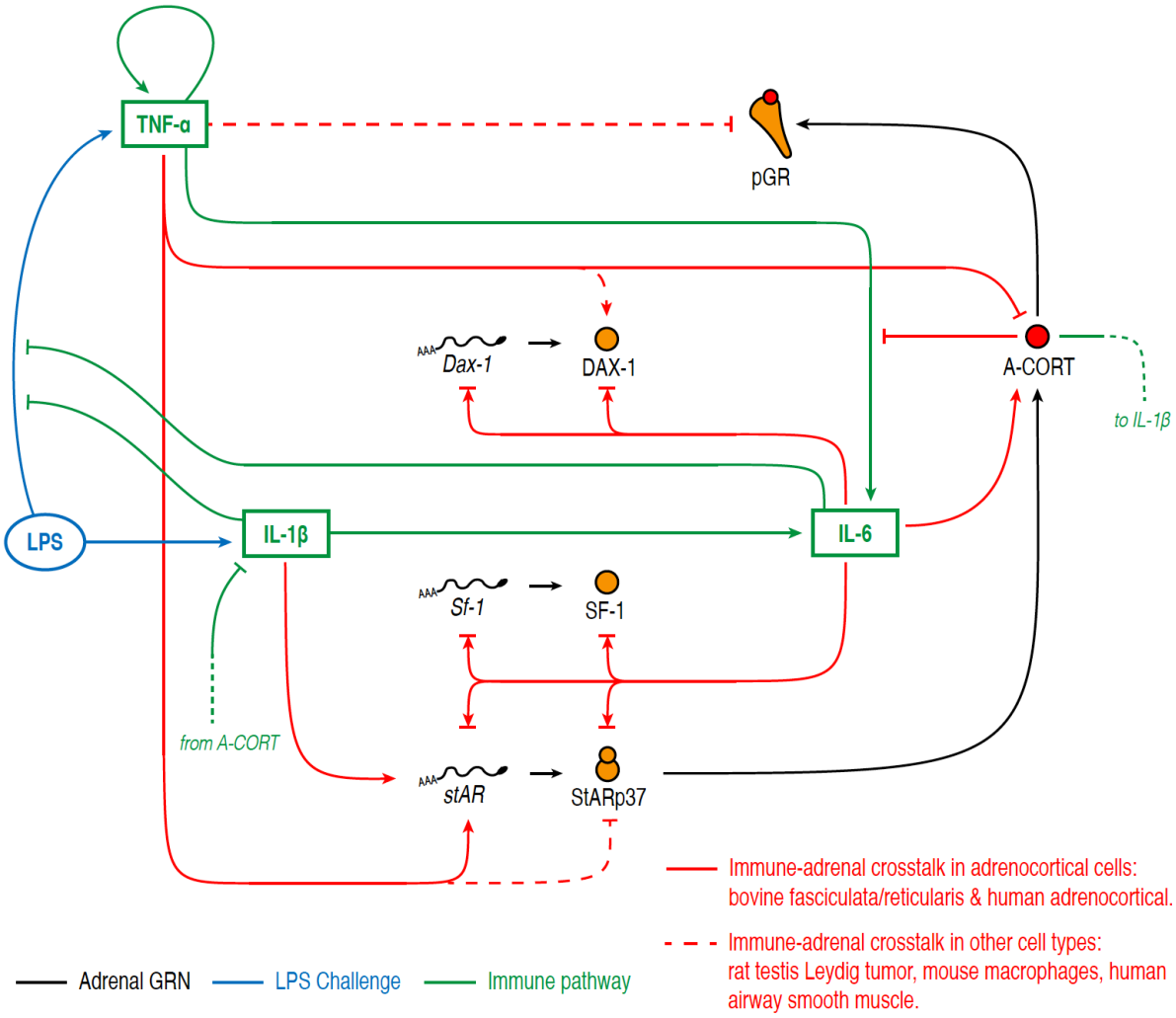

Fig. S8. Cross-talk between the SRN and the immune pathway. During the inflammatory response elicited by LPS, the synthesis of glucocorticoids in adrenocortical cells is modulated by the immune pathway through cytokines. The SRN, in turn, also feeds back upon these cytokines, thus exhibiting cross-talk between both regulatory networks.

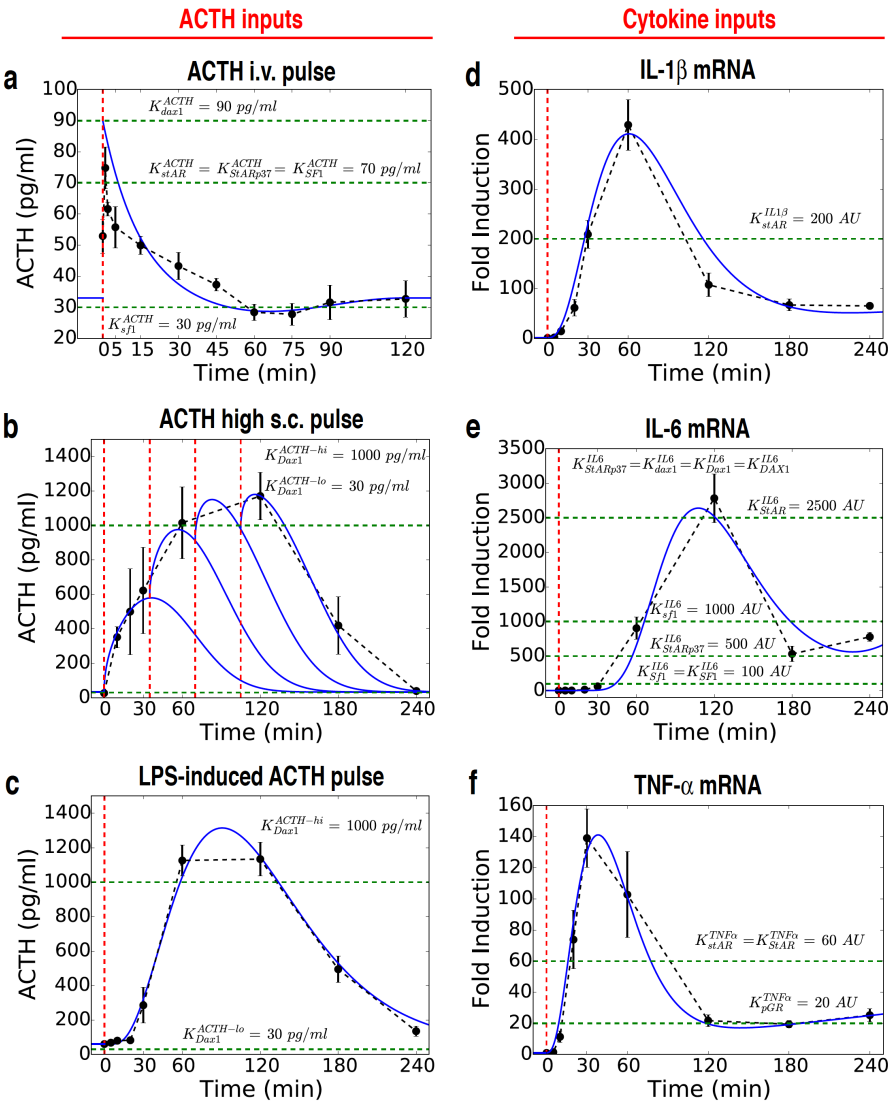

Fig. S9. ACTH and cytokine "virtual" pulse input functions used in the computer simulations and their associated sensitivities. (a) Small pulse (low dose) of ACTH, **(b)** large pulse of ACTH integrated by four cumulative doses, **(c)** large pulse of ACTH elicited by LPS, **(d-f)** cytokine pulses elicited by LPS.

Supplementary Tables

Supplementary Table 1. Primer Sequences.

Target	Forward Primer	Reverse Primer
CYP11A1 hnRNA	TGTGTGTGTGACCCCAGGAGAC	CCCAGGTCCTGCTTGAGAGGCT
CYP11A1 mRNA	TGCGAGGGTCCTAACCCGGA	ACCTTCCAGCAGGGGCACGA
DAX-1 hnRNA	TCCAGGCCATCAAGAGTTTC	AAGCTCACCCACTTGACCAC
DAX-1 mRNA	TCCAGGCCATCAAGAGTTTC	GTGCTCAGTGAGGATCTGC
GAPDH mRNA	CCATCACTGCCACCCAGAAGA	GACACATTGGGGGTAGGAACA
HSL hnRNA	AGGTAGGAGCTGTACCCCTG	CTGCAAAGACGTTGGACAGC
HSL mRNA	TATCCGCTCTCCGGTTGA	CGAGCACTGGAGGAGTGTTT
IL-1β hnRNA	AGTTGTCCGTGTGTATGGGATG	GCCAGGCAGAAAGGTTTTTGTT
IL-1β mRNA	ACCTATGTCTTGCCCGTGGA	AGGTCGTCATCATCCCACGA
IL-6 hnRNA	CCCAGAGCACTCCACAAGG	TCTTGGTCCTTAGCCACTCCT
IL-6 mRNA	AGCCACTGCCTTCCCTACTT	GCCATTGCACAACTCTTTTCTCA
MC2R hnRNA	GAAGTCCGTGAGGTTGSACA	TTGTGCGGAAGGATCCAGTTT
MC2R mRNA	GCTTTTGATCCCTGCTTTGAGTG	CATCTGTTAAAGAAGGAAAGGCTGG
MRAP hnRNA	ACCTCATTCCTGTGGACGAG	ACCCGCCATATTATCACTGC
MRAP mRNA	CCTCCCGGTGTGTGGCCTCT	GGGGACTATGCCTTACCTGTGGGG
NR4A1 hnRNA	CTTGTGGGGTCCCTGCCTGC	ACGTGGAGAAGGGGCGGTCT
NR4A1 mRNA	GCGGAACCGCTGCCAGTTCT	GCATCTGGGGGCTGCTTGGG
SF-1 hnRNA	AGAGGGTGATGGGCTGCT	ACCTCCACCAGGCACAATAG
SF-1 mRNA	CGCCAGGAGTTTGTCTGTCT	ACCTCCACCAGGCACAATAG
StAR hnRNA	GCAGCAGCAACTGCAGCACTAC	GTGCCCCCGGAGACTCACCT
StAR mRNA	CTGGCAGGCATGGCCACACA	GGCAGCCACCCCTTGAGGTC
TNF-α hnRNA	CCGTGACTGTAATCGCCCTAC	CTTTAGGAGGCTGCAGAGAGAC
TNF-α mRNA	AAATGGGCTCCCTCTATCAGTTC	TCTGCTTGGTGGTTTGCTACGAC

Supplementary Table 2. Statistical information (P values). Related to Figs. 2–4, 6, and to Figs. S3,5,6.

Component	P value		
	Fig. 2 and Fig. S3	Fig. 3 and Fig. S5	Figs. 4, 6 and Fig. S6
ACTH	<0.0001	0.002	<0.0001
A-CORT	<0.0001	<0.0001	<0.0001
P-CORT	<0.0001	<0.0001	<0.0001
pHSL-(Ser660)	<0.0001	0.001	<0.0001
pHSL-(Ser563)	<0.0001	0.003	<0.0001
pCREB	0.001	0.028	<0.0001
StAR hnRNA	<0.0001	0.001	<0.0001
StAR mRNA	0.067	<0.0001	<0.0001
CYP11A1 hnRNA	<0.0001	0.002	0.007
CYP11A1 mRNA	0.013	0.051	<0.0001
MRAP hnRNA	<0.0001	<0.0001	<0.0001
MRAP mRNA	<0.0001	<0.0001	<0.0001
MC2R hnRNA	0.016	0.051	0.002
MC2R mRNA	<0.0001	0.002	<0.0001
HSL hnRNA	0.517	0.16	0.006
HSL mRNA	0.221	0.021	<0.0001
Nur77 hnRNA	<0.0001	<0.0001	<0.0001
Nur77 mRNA	<0.0001	<0.0001	<0.0001
SF-1 hnRNA	0.008	0.003	0.005
SF-1 mRNA	0.361	0.002	0.091
DAX-1 hnRNA	0.001	0.001	0.001
DAX-1 mRNA	0.154	0.002	<0.0001
StARp37	0.755	0.441	<0.0001
StARp32	0.967	0.457	<0.0001
StARp30	0.354	0.007	0.433
CYP11A1	0.482	0.814	0.971
HSL	0.777	0.993	0.146
SF-1	0.385	0.492	0.76
DAX-1	0.728	0.301	0.003
pGR	0.032	0.003	0.528

Supplementary Materials and Methods

Animals

All experiments were conducted on adult male Sprague–Dawley rats (Harlan Laboratories, Inc., Blackthorn, UK) weighting 220-250g at the time of arrival. Animals were given a 1-week acclimatization period prior to the start of the experiments, they were maintained under a 14 h light, 10 h dark schedule (lights on at 0500 h), and housed four per cage with ad libitum access to food and water. All animal procedures were approved by the University of Bristol Ethical Review Group and were conducted in accordance with Home Office guidelines and the United Kingdom Animals (Scientific Procedures) Act, 1986.

Surgery

Rats were anaesthetised using isoflurane and an indwelling catheter was inserted in the right jugular vein as previously described (Spiga et al., 2007). In brief, the right jugular vein was exposed, and a silastic-tipped (Merck, Whitehouse, NJ) polythene cannula (Portex, Hythe, UK) was inserted into the vessel to allow substance infusion. Cannula was prefilled with pyrogen-free heparinized (10 IU/ml) isotonic saline; the free end was exteriorized through a scalp incision and then tunnelled through a protective spring that was anchored to the parietal bones using two stainless steel screws and self-curing dental acrylic. For the high dose ACTH experiment, in addition to the intravenous cannula, during the same surgery a subcutaneous cannula was implanted under the skin between the shoulder blades. After recovery, animals were housed in individual cages in a soundproof room. The end of the protective spring was attached to a mechanical swivel that rotated through 360° in a horizontal plane and 180° through a vertical plane, allowing the rats to maximize freedom of movement. The cannula was flushed daily with heparinized saline to maintain patency.

Experiments and tissue collection

All experiments started at 9 AM and were performed 5–7 days after the surgery. *ACTH pulse experiment.* To investigate the dynamic adrenal response to an ACTH pulse rats were given an intravenous injection of synthetic ACTH (10 ng per 0.1 ml, i.v.; Synachten, Alliance Pharma, Cheltenam, United Kingdom). *High dose ACTH experiment*. To investigate the effect of a high dose of ACTH, that is able to produce similar plasma ACTH levels as observed after LPSs treatment, rats were given four injections of ACTH (2 µg/kg, sc; Synachten Depot, AlliancePharma, Cheltenam, United Kingdom) at 35-minute intervals, as previously described in (Gibbison et al., 2015). *LPS experiment*. To investigate the dynamic

adrenal response to an inflammatory stress rats were given an intravenous injection of LPS (Escherichia coli, clone 055:B5; 25 µg/rat in 0.1 mL of sterile saline; Sigma, Dorset, United Kingdom).

At the end of each experiment, rats were overdosed with 0.2 mL of sodium pentobarbitone (Euthatal, 200 mg/mL; Merial, Harlow, United Kingdom) at specific time points shown in the figures. Trunk blood was collected in ice-cold tubes containing EDTA (0.5 M; pH 7.4) and Trasylol (Aprotinin, 500,000 KIU/mL, Roche Diagnostics). Plasma was separated by centrifugation and then stored at –80°C until processed for ACTH and corticosterone measurement.

Adrenal glands were collected and the inner zones (comprising the *zona fasciculata* and the *zona reticularis* of the cortex and the adrenal medulla) were separated from the outer zone (containing the *zona glomerulosa* and the *capsula*). Individual inner zones were immediately frozen until processing for isolation of RNA for real-time quantitative polymerase chain reaction (RTqPCR; left adrenal), and for protein extraction for Western immunoblotting and corticosterone measurement (right adrenal) as previously described (Park et al., 2013; Spiga et al., 2011b).

RNA isolation and RT-qPCR

Total RNA was extracted from the inner zone of individual adrenals using TRIzol reagent (Invitrogen, Hopkinton, MA, USA), followed by purification using RNeasy mini kit reagents, and column DNase digestion (Qiagen, Valencia, CA, USA) to remove genomic DNA contamination. Complementary DNA was reverse transcribed from 1 µg of total RNA using Cloned AMV First-Strand cDNA synthesis kit (Invitrogen). Primers were designed to specifically detect primary transcript (hnRNA) or mRNA (Table S1). Fast SYBRGreen Master (Applied Biosystems, Foster City, CA, USA) was used for the amplification mixture with each primer at a final concentration of 200 nm and 2 µl of cDNA for a total reaction volume of 25 µl. PCR reactions were performed on a spectrofluorometric thermal cycler. The expression of each target gene was normalized to glyceraldehyde 3-phosphate dehydrogenase (GAPDH) mRNA as determined in a separate real-time PCR reaction. The absence of RNA detection when the reverse transcription step was omitted indicated the lack of genomic DNA contamination in the RNA samples.

Western immunoblotting

Whole cell lysate from the inner zone of individual adrenals were prepared using RIPA buffer (Sigma) supplemented with 0.2 mM Na orthovanadate, 2 mM NaF, and Complete Protease

Inhibitor (Roche Diagnostics Ltd., Burgess Hill, UK). Protein concentration was quantified by spectrophotometry using the Pierce BCA protein assays, (Thermo Fisher Scientific Inc. Rockford, IL, USA). Aliquots of each sample (10–15 µg of protein) were loaded and separated in a 10% or 4–15% Tris–Glycine gel (BioRad, Hercules, CA, USA), transferred to a PVD membrane (GE Amersham Biosciences, Piscataway, NJ, USA), blocked with 5% non-fat milk or 1% bovine serum albumin (BSA, sigma) in 1 × Tris-buffered saline plus 0.05% Tween 20 (TBST) and incubated overnight with Aliquots of each sample (10–15 µg of protein) were loaded and separated in a 10% or 4–15% Tris–Glycine gel (BioRad, Hercules, CA, USA), transferred to a PVD membrane (GE Amersham Biosciences, Piscataway, NJ, USA), blocked with 5% non-fat milk or 1% bovine serum albumin (BSA, sigma) in 1 × Tris-buffered saline plus 0.05% Tween 20 (TBST) and incubated overnight with antibodies to StAR, DAX-1, CYP11A1, HSL, GR (Santa Cruz Biotechnologies, Inc., Dallas, TX, US), SF-1 (Upstate Biotechnlogies Inc., Lake Placid, NY, US); CREB, phospho-CREB(Ser133), phospho-HSL(Ser660), phospho-HSL(Ser563); phospho-GR(Ser211) (Cell Signalling Technology, Danvers, MA, US).

After washing with TBST, the membranes were incubated with a horseradish peroxidase-conjugated donkey anti-rabbit IgG or donkey anti-goat IgG (Santa Cruz Biotechnologies). Immunoreactive bands were visualized using ECL Plus TM reagents (GE Amersham Biosciences) followed by exposure to BioMax MR film (Eastman Kodak; Rochester, NY, USA). After film exposure, blots were stripped and assayed for anti-goat vinculin (Santa Cruz Biotechnology). The intensity of the protein targets bands integrated with the area was quantified using a computer image analysis system, Image J (developed at the National Institutes of Health and freely available at: http://rsb.info.nih.gov). Data points for each gene were then normalized relative to the vinculin band in the respective sample.

Hormone measurement

Adrenal CORT was measured in adrenal whole cell extract prepared for Western blotting and CORT levels were normalized to the total protein content. Total plasma and adrenal CORT was measured by radioimmunoassay (RIA) using a citrate buffer (pH 3.0) to denature the binding globulin as previously described (Spiga et al., 2007). Antiserum was kindly supplied by Professor Gabor Makara (Institute of Experimental Medicine, Budapest, Hungary) and [125I] CORT was purchased from Izotop (Budapest, Hungary). ACTH in plasma was measured by RIA using a commercially available assay (MP Biomedicals, Santa Ana, California, USA) in accordance with the manufacturer's instructions.

Statistics

Sample sizes in each experiment were determined on the basis of pilot studies and previous experience with similar experimental design. Animals were allocated to each experimental group (time point after treatment) by simple randomization. Experimenters were blinded to the experimental group at the time of hormones, RNA and protein measurements.

Data are represented as the mean ± SEM, hnRNA, mRNA and protein data are expressed as fold induction of basal (time 0). No animals or samples were excluded from statistical analysis. To check data for normality and equality of variance, we used Shapiro-Wilk and Leven tests, respectively. The overall effect of treatments was analysed using the Independent-Samples Kruskal-Wallis Test. Asymptotic significances for each experiment are shown in Table S2. Statistical significance was set at $P < 0.05$.

Mathematical Model

Contents

1 Model Development

The adrenal SRN controlling the CORT biosynthetic pathway is very complex (Fig. S1). In order to develop a useful yet, manageable mathematical model, we simplified the network by reducing the number of components to a minimum (Fig. 1). Our model predictions support these gene components as the core regulatory clockwork of the SRN. A list of source references to the connections between nodes in both the full and reduced network is shown in Table A.

The mathematical model is representative of a single adrenocortical cell stimulated by an ACTH input. Specifically, ACTH stimulates adrenocortical cells for controlling the biosynthesis of CORT, which, respectively, represent the 'input' and 'output' of the SRN. Since our model is decoupled from other components of the HPA axis, we reproduced endogenous ACTH levels originated from the brain by using an ultradian oscillatory input (T = 75 min) with circadian modulated amplitude. Thus, in basal, non-stressed conditions, the model dynamics is not static but exhibits an ultradian and circadian rhythmicity driven by the ACTH input. Some model assumptions and biological considerations are the following:

i) The model doesn't focus on the specifics of the CORT biosynthetic pathway within the mitochondria or its release into the bloodstream. Instead, we consider A-CORT as a better readout of the network since its increase occurs earlier than P-CORT, thus reflecting the very first product of CORT biosynthesis.

ii) The network architecture emphasises the crosstalk between StAR, DAX-1 and SF-1 genes. For each of these genes, their hnRNA, mRNA and protein species are modelled explicitly. Though MC2R, MRAP, Nur77 and HSL genes are included in the full network map (Fig. S1), the network architecture suggests they're not directly involved in feedback regulation within the genomic pathway.

iii) Likewise, even though the dynamics of the different phosphorylation states of the HSL protein (pHSL-S565, pHSL-S563 and pHSL-S660) is important to understand cholesterol synthesis, it is StARp37 the one controlling the mitochondrial import of cholesterol, which is the rate-limiting step for ACORT biosynthesis. Accordingly, we didn't include the pHSL dynamics in the present model.

iv) To decouple the intra-adrenal system from the whole HPA axis, we assumed ACTH as an externally controlled input that targets specific components within the adrenal SRN. This took the form of either an endogenous ultradian input with circadian amplitude, a single pulse perturbation, or a combination of both.

Furthermore, we simplified the model by reducing the number of model equations. For instance, cAMP, PKA and pCREB intermediary species in the signalling cascade ending in promoter regulation are not modelled explicitly. Though pCREB is known to regulate transcription of StAR [Manna et al., 2009; Sugawara et al., 1997a,b; Zhao et al., 2005] as well as of other steroidogenic genes, the components of the cascade are known to be downstream of the ACTH pathway, which is already considered in the model.

To reproduce experimental conditions, we administered "virtual" ACTH pulses near the circadian nadir of the endogenous ACTH oscillations. Specifically, we simulated 7 pulses, one every 10 min, distributed between 8 AM and 9 AM of the day. The dynamics during the 120 min following the stimuli was recorded and averaged for the ACTH i.v. pulse experiments, and during 240 min for the high s.c. ACTH and LPS challenge experiments.

1.1 DAX-1 Gene Expression

The dynamics of gene activation, represented by the newly synthesised, non-edited hnRNA $dax1$[1], can be represented by the following equation:

$$\dot{dax}1 = \sigma_{dax1} + k_{dax1} f_{dax1}(SF1, pGR) g^{-}_{dax1}(ACTH) - \gamma_{dax1} dax1 \tag{1}$$

where σ_{dax1} is the basal transcription rate, k_{dax1} is the maximum transcription rate, γ_{dax1} is the $dax1$ hnRNA degradation rate, and f_{dax1} is a function accounting for $dax1$ transcription initiation by the synergistic action of SF1 and pGR, which is modulated by ACTH. Since the specific molecular mechanisms governing the Dax1[2] promoter activation are still poorly understood, we take an heuristic approach and propose a phenomenological function that captures the effects observed in the study by [Gummow et al., 2006], in which SF1 and GR were cotransfected with a Dax1-Luc reporter into JEG3 cells and stimulated with varying doses of dexamethasone (thus mimicking steroid activation of the GR). Subsequently, a similar experiment was performed in Y1 cells which were concomitantly stimulated with ACTH to assess the level of induction when SF1 and GR were present separately or simultanouesly.

CORT-activated GR, which we measured via its phosphorylated form pGR, is known to synergise with SF1 to enhance Dax1 gene expression (up to 30-fold activation in a dose-dependent dexamethasone stimulation experiment). In addition, SF1 is known to also activate the promoter in a pGR-independent way (11-fold activation). Moreover, Glucocorticoid Responsive Elements (GREs) have been identified in the Dax1 promoter and they are dose-responsive to dexamethasone stimulation in the absence of SF1 [Gummow et al., 2006]. However, we will not consider SF1-independent effects on f_{dax1} as the elicited fold activation is not only very close to baseline but also small when compared against SF1-pGR synergistic activation and SF1-dependent induction. Further experiments performed by [Gummow et al., 2006] suggest that SF1 and pGR form a molecular complex at the Dax1 promoter which enhances its expression upon steroid stimulation. Considering this and the role that SF1 has in regulating the expression of the StAR gene after binding to the DAX1 protein (thus forming another molecular complex) [Sugawara et al., 1997a,b; Fan et al., 2004; Gummow et al., 2006; Manna et al., 2009], we propose that f_{dax1} takes the form:

$$f_{dax1}(SF1, pGR) = \frac{\frac{SF1}{K_{SF1}} + \frac{SF1 \cdot pGR}{K_{SF1} \cdot K_G}}{1 + \frac{SF1}{K_{SF1}} + \frac{SF1 \cdot pGR}{K_{SF1} \cdot K_G}} \tag{2}$$

In Eq. 2, it can be seen that SF1 is necessary for activating the Dax1 promoter, either independently (i.e. in its free form) or forming a complex with pGR. Thus, pGR can be viewed as an enhancer which acts upon Dax1 promoter through the SF1-pGR complex. The non-linearity observed in Eq. 2 is expected from the pGR-independent SF1 binding to any of its three binding sites within the Dax1 promoter and from the synergy between the central SF1 binding site and the proximal GRE binding site that enhances expression [Gummow et al., 2006]. As the specific mechanisms of regulation are unknown, we chose the simplest empirical representation of the Dax1 promoter regulation by SF1 and pGR transcription factors.

Furthermore, [Gummow et al., 2006] also show that both the SF1 and SF1-pGR synergistic activation of the Dax1 promoter are decreased upon ACTH stimulation. We modelled this by multiplying the second term in Eq. 1 by a decreasing function $g^{-}_{dax1}(ACTH)$. As the specific mechanisms and molecular intermediaries of ACTH-dependent modulation are unknown, it is convenient to choose a non-linear Hill type function (see Eq. 3). The K's in Eqs. 1 and 2 account for half-maximum constants which were determined by fitting the model to data.

$$g^{-}_{dax1}(ACTH) = \frac{K^{ACTH^4}_{dax1}}{K^{ACTH^4}_{dax1} + ACTH^4} \tag{3}$$

[1]The hyphen in *dax-1*, *Dax-1*, *DAX-1*, *sf-1*, *Sf-1*, *SF-1*, and *A-CORT* labels was dropped to avoid confusion with a minus sign.

[2]In what follows, the non-italicised nomenclature will be used for gene names unless otherwise specified, whereas the italicised will be reserved for state variables used in the mathematical model (e.g. $dax1$, $Dax1$, and $DAX1$ refer, respectively, to hnRNA, mRNA, and protein concentrations).

The mature transcript dynamics is given by

$$\dot{Dax1} = k_{Dax1} dax1_{\tau_{Dax1}} - \gamma_{Dax1} Dax1 \cdot g^{\mp}_{Dax1}(ACTH) \tag{4}$$

where k_{Dax1} stands for the mRNA maturation rate and γ_{Dax1} is the mRNA degradation rate. RT-PCR experiments aimed at detecting hnRNA can't distinguish the transcriptional stage at which the RNA is within the nucleus. However, we know that edition processes such as splicing have finished once mature mRNAs are detected. Hence, we assumed Eq. 4 is delayed by τ_{Dax1}, which accounts for the elapsed time since transcription initiation up to the emergence of a hnRNA plus the maturation time after completion of transcription (splicing, capping, polyadenylation and mRNA nuclear export processes).

In addition, high doses of ACTH are known to destabilise $Dax1$ transcripts [Ragazzon et al., 2006], which in a first instance was modelled by multiplying the turnover term in Eq. 4 by a positively increasing function of ACTH ($g^{+}_{Dax1}(ACTH)$). However, when re-calibrating the model by fitting it to our ACTH i.v. pulse experiments, we observed a mismatch between its predictions and our DAX1 mRNA and protein data. We realised that our assumption of a monotonously-increasing function was based on experimental results by [Ragazzon et al., 2006] that were performed using very high levels of ACTH. Thus, to fit our model to data from low ACTH i.v. pulse experiments, but keeping consistency with previous observations by [Ragazzon et al., 2006] at high ACTH levels, we hypothesised an ACTH dose-dependent control mechanism of $Dax1$ mRNA stability that was modelled assuming its turnover rate is modulated by the function $g^{\mp}_{Dax1}(ACTH)$. Though it's not clear how ACTH actually promotes or inhibits degradation of $Dax1$, we propose that a non-monotonous regulatory function would provide the best fit of the model to our experimental data in both the low and high ACTH *stimuli* experiments. We model this through a decreasing-then-increasing function containing two half-maximum constants: $K^{ACTH-lo}_{Dax1}$ for inhibition at low doses of ACTH, and $K^{ACTH-hi}_{Dax1}$ for activation at high doses of ACTH (Fig. S4). This function takes the form:

$$g^{\mp}_{Dax1}(ACTH) = \frac{K^{ACTH-lo}_{Dax1}}{K^{ACTH-lo}_{Dax1} + ACTH} + \frac{ACTH}{K^{ACTH-hi}_{Dax1} + ACTH} \tag{5}$$

Finally, the DAX1 protein dynamics is governed by:

$$\dot{DAX1} = k_{DAX1} Dax1_{\tau_{DAX1}} - \gamma_{DAX1} DAX1 \tag{6}$$

where k_{DAX1} stands for the protein translation rate, τ_{DAX1} is the delay associated to translation, and γ_{DAX1} is the protein degradation rate.

1.2 SF-1 Gene Expression

The dynamics of gene activation, represented by the newly synthesised, non-edited $sf1$ hnRNA, can be represented by the following equation:

$$\dot{sf1} = \sigma_{sf1} + k_{sf1} g^{+}_{sf1}(ACTH) - \gamma_{sf1} sf1 \tag{7}$$

where σ_{sf1} is the basal transcription rate, k_{sf1} is the maximum transcription initiation rate, and γ_{sf1} is the $sf1$ degradation rate. To the best of our knowledge, the SF1 gene is not subject to transcriptional regulation by any of the proteins considered in the model. Thus, conversely to Eq. 1, here we have no function accounting for $sf1$ transcription modulation by any transcription factors other than the effects induced by ACTH. This is modelled by a function $g^{+}_{sf1}(ACTH)$, which takes the form:

$$g^{+}_{sf1}(ACTH) = \frac{ACTH^4}{K^{ACTH^4}_{sf1} + ACTH^4} \tag{8}$$

Though in our model we consider that SF1 gene expression is regulated by ACTH alone [Ragazzon et al., 2006], regulation by other transcription factors within the steroidogenic pathway cannot be ruled out. This poses interesting questions about the role of this gene in controlling the adrenal

response. Moreover, evidence suggests that its mRNA and protein levels remain constant after variations in cAMP concentration, which is a known mediator of the ACTH pathway [Fan et al., 2004].

The mature transcript dynamics is given by:

$$\dot{Sf1} = k_{Sf1} sf1_{\tau_{Sf1}} - \gamma_{Sf1} g_{Sf1}(Sf1) \tag{9}$$

where k_{Sf1} stands for the mRNA maturation rate and γ_{Sf1} is the mRNA degradation rate. By similar arguments as in Eq. 4, we assumed Eq. 9 is delayed by τ_{Sf1}. Importantly, we found out that the best fit of the model to our data was achieved when assuming a Michaelis-Menten degradation of $Sf1$ mRNA. Thus, the function $h_{Sf1}(Sf1)$ takes the form:

$$h_{Sf1}(Sf1) = \frac{Sf1}{K_{Sf1} + Sf1} \tag{10}$$

Finally, the $SF1$ protein dynamics is governed by:

$$\dot{SF1} = k_{SF1} Sf1_{\tau_{SF1}} - \gamma_{SF1} SF1 \cdot g^{-}_{SF1}(ACTH) \tag{11}$$

where k_{SF1} stands for the protein translation rate, τ_{SF1} is the delay associated to translation, and γ_{SF1} is the protein degradation rate. Since ACTH is suspected to stabilise $SF1$, probably through phosphorylation or ubiquitination of the proteasome [Æsøy et al., 2002], we assume its turnover rate is modulated by a function $g^{-}_{SF1}(ACTH)$, which takes the form:

$$g^{-}_{SF1}(ACTH) = \frac{K^{ACTH}_{SF1}}{K^{ACTH}_{SF1} + ACTH} \tag{12}$$

1.3 StAR Gene Expression

The dynamics of StAR gene activation, represented by the newly synthesised, non-edited $stAR$ hnRNA, can be represented by the equation:

$$\dot{stAR} = \sigma_{stAR} + k_{stAR} f_{stAR}(SF1, DAX1) g^{+}_{stAR}(ACTH) - \gamma_{stAR} stAR \tag{13}$$

where σ_{stAR} is the basal transcription rate, k_{stAR} is the maximum transcription initiation rate, γ_{stAR} is the $stAR$ degradation rate, and f_{stAR} is a function accounting for $stAR$ transcription initiation controlled positively by $SF1$ and negatively by $DAX1$. This $DAX1$-mediated steroidogenic inhibition follows from the finding that $DAX1$ inhibits $SF1$ transactivation upon binding it [Babu et al., 2002; Fan et al., 2004], thus preventing StAR gene activation. In addition, ACTH is known to control the StAR gene activation directly through pCREB [Sugawara et al., 1997a,b; Manna et al., 2009]. However, since we're not modelling pCREB explicitly, we employ the function $g^{+}_{stAR}(ACTH)$ to model the StAR gene activation by ACTH. This function takes the form:

$$g^{+}_{stAR}(ACTH) = \frac{ACTH^4}{K^{ACTH^4}_{stAR} + ACTH^4} \tag{14}$$

In summary, an $SF1$ dependent activation mechanism, similar to the one modelled in Eq. 2, has been shown to be responsible for StAR gene activation [Sugawara et al., 1997b; Manna et al., 2003; Fan et al., 2004; Xu et al., 2009]. This follows from cotransfection experiments carried out by [Fan et al., 2004] to explore the effects of $SF1$ (a.k.a. Ad4BP) and $DAX1$ concomitantly with Forskolin stimulation of the PKA pathway.

These considerations were taken into account to assume that f_{stAR} takes the form:

$$f_{stAR}(SF1, DAX1) = \frac{\frac{SF1}{K_{SF1}}}{1 + \frac{SF1}{K_{SF1}} + \frac{DAX1}{K_D}} \tag{15}$$

In Eq. 13, it can be seen that both ACTH and $SF1$ are necessary for activating $stAR$, whereas $DAX1$ modulates the promoter activity by binding to $SF1$ at the promoter site (the gene is inactive

if either ACTH or $SF1$ are absent, but not if $DAX1$ is). Importantly, this empirical approach facilitates modifying Eq. 15 if we wish to account for $DAX1$ dosage dependent effects observed in diseased states [Xu et al., 2009; Sadasivam et al., 2015]. Just as in Eq. 2, the K's in Eq. 15 account for half-maximum constants (often interpreted as sensitivities) and were determined by fitting the model to data.

The mature transcript dynamics is given by:

$$\dot{StAR} = k_{StAR} stAR_{\tau_{StAR}} - \gamma_{StAR} h_{StAR}(StAR) \tag{16}$$

where k_{StAR} stands for the mRNA maturation rate and γ_{StAR} is the mRNA degradation rate. By similar arguments as in Eq. 4, we assumed Eq. 16 is delayed by τ_{StAR}. Importantly, we found out that the best fit of the model to data was achieved when assuming a Michaelis-Menten degradation of $StAR$ mRNA. Thus, the function $h_{StAR}(StAR)$ takes the form:

$$h_{StAR}(StAR) = \frac{StAR}{K_{StAR} + StAR} \tag{17}$$

Finally, for the StAR protein dynamics we will account for the 37 kDa precursor, as it has been shown to be the one responsible for cholesterol import before being itself cleaved and imported to the mitochondria [Arakane et al., 1998; Bose et al., 2002; Manna et al., 2009]. It's dynamics is given by:

$$\dot{StARp37} = k_{StARp37} StAR_{\tau_{StARp37}} - \mu_{StARp37} StARp37 g^{-}_{StARp37}(ACTH) \tag{18}$$

where $k_{StARp37}$ stands for the protein translation rate, $\tau_{StARp37}$ is the delay associated to translation, and $\mu_{StARp37} = \gamma_{StARp37} + \epsilon_{StARp37}$ is the $StARp37$ turnover rate. This value accounts for the proteasome-mediated degradation rate of the active precursor $StARp37$, $\gamma_{StARp37}$, and the import rate of the $StARp37$ cleaved byproducts into mitochondria, $\epsilon_{StARp37}$ [Arakane et al., 1997; Bose et al., 2002; Manna et al., 2009]. As it has been show that $StARp37$ activity is proportional to its residence time in the cytosol [Bose et al., 2002; Granot et al., 2003], and that PKA-mediated phosphorylation stabilises the precursor [Clark and Hudson, 2015], we have included the function $g^{-}_{StARp37}(ACTH)$ in the turnover term in Eq. 18, which takes the form:

$$g^{-}_{StARp37}(ACTH) = \frac{{K^{ACTH}_{StARp37}}^4}{{K^{ACTH}_{StARp37}}^4 + ACTH^4} \tag{19}$$

1.4 A-CORT Dynamics

As mentioned before, the CORT biosynthetic pathway within the mitochondria won't be modelled explicitly at this stage. Instead, we assume that $ACORT$ dynamics is governed by:

$$\dot{ACORT} = k_{ACORT} f_{ACORT}(StARp37) - \mu_{ACORT} ACORT \tag{20}$$

where k_{ACORT} is the maximum synthesis rate of ACORT, and the turnover term $\mu_{ACORT} = \gamma_{ACORT} + \epsilon_{ACORT}$ accounts for the ACORT degradation rate γ_{ACORT} and the export rate from the adrenal cell into the bloodstream ϵ_{ACORT}. The function f_{ACORT} expresses the dependence of ACORT synthesis on the precursor $StARp37$ and takes the form:

$$f_{ACORT}(StARp37) = \frac{StARp37}{K_{StARp37} + StARp37} \tag{21}$$

where the big K has the same meaning as in previous functions and was determined by fitting the model to data. As mentioned before, $StARp37$ controls the import of cholesterol into the mitochondria [Bose et al., 2002], which is the rate limiting step for corticosteroid biosynthesis. We assumed this process can be represented as a Michaelis-Menten reaction (see Eq. 21) [Arakane et al., 1997; Manna et al., 2009; Spiga et al., 2014]. Importantly, although $StARp37$ is downstream of ACTH (through regulation of the StAR gene), ACORT is known to respond to ACTH stimulation on a much shorter timescale than the time needed for ACTH to exert its effects on $StARp37$ through the cAMP/PKA/pCREB pathway. This likely happens due to PKA mediated $StARp37$ stabilisation in the cytosol upon ACTH stimulation [Arakane et al., 1997; Manna et al., 2009], a process that is already accounted for in the turnover term in Eq. 18.

1.5 pGR Dynamics

Lastly, instead of modelling the concentration of the glucocorticoid receptor, we model the measured levels of its phosphorylated form pGR, a marker of its activity. We propose the dynamics of the pGR is governed by:

$$\dot{pGR} = k_{GR} f_{pGR}(ACORT) - \gamma_{pGR} pGR \tag{22}$$

where k_{pGR} stands for the pGR activation rate by ACORT and γ_{pGR} is it's deactivation rate. The function f_{pGR} takes the form:

$$f_{pGR}(ACORT) = \frac{ACORT}{K_{ACORT} + ACORT} \tag{23}$$

where K_{ACORT} stands for the half-maximum constant of pGR activation by ACORT.

1.6 Model Equations for the SRN

The complete set of model equations is shown below:

$$\begin{aligned}
\dot{dax1} &= \sigma_{dax1} + k_{dax1} f_{dax1}(SF1, pGR) g^{-}_{dax1}(ACTH) - \gamma_{dax1} dax1,\\
\dot{Dax1} &= k_{Dax1} dax1_{\tau_{Dax1}} - \gamma_{Dax1} Dax1 g^{\mp}_{Dax1}(ACTH),\\
\dot{DAX1} &= k_{DAX1} Dax1_{\tau_{DAX1}} - \gamma_{DAX1} DAX1,\\
\dot{sf1} &= \sigma_{sf1} + k_{sf1} g^{+}_{sf1}(ACTH) - \gamma_{sf1} sf1,\\
\dot{Sf1} &= k_{Sf1} sf1_{\tau_{Sf1}} - \gamma_{Sf1} h_{Sf1}(Sf1),\\
\dot{SF1} &= k_{SF1} Sf1_{\tau_{SF1}} - \gamma_{SF1} SF1 g^{-}_{SF1}(ACTH),\\
\dot{stAR} &= \sigma_{stAR} + k_{stAR} f_{stAR}(SF1, DAX1) g^{+}_{stAR}(ACTH) - \gamma_{stAR} stAR,\\
\dot{StAR} &= k_{StAR} stAR_{\tau_{StAR}} - \gamma_{StAR} h_{StAR}(StAR),\\
\dot{StARp37} &= k_{StARp37} StAR_{\tau_{StARp37}} - \mu_{StARp37} StARp37 g^{-}_{StARp37}(ACTH),\\
\dot{ACORT} &= k_{ACORT} f_{ACORT}(StARp37) - \mu_{ACORT} ACORT,\\
\dot{pGR} &= k_{GR} f_{pGR}(ACORT) - \gamma_{pGR} pGR.
\end{aligned}$$

where:

$$\begin{aligned}
g^{-}_{dax1}(ACTH) &= \frac{K^{ACTH^4}_{dax1}}{K^{ACTH^4}_{dax1} + ACTH^4},\\
g^{\mp}_{Dax1}(ACTH) &= \frac{K^{ACTH-lo}_{Dax1}}{K^{ACTH-lo}_{Dax1} + ACTH} + \frac{ACTH}{K^{ACTH-hi}_{Dax1} + ACTH},
\end{aligned}$$

$$g^{+}_{sf1}(ACTH) = \frac{ACTH^4}{K^{ACTH^4}_{sf1} + ACTH^4}, \qquad g^{-}_{SF1}(ACTH) = \frac{K^{ACTH}_{SF1}}{K^{ACTH}_{SF1} + ACTH},$$

$$g^{+}_{stAR}(ACTH) = \frac{ACTH^4}{K^{ACTH^4}_{stAR} + ACTH^4}, \qquad g^{-}_{StARp37}(ACTH) = \frac{K^{ACTH}_{StARp37}{}^4}{K^{ACTH}_{StARp37}{}^4 + ACTH^4},$$

$$h_{Sf1}(Sf1) = \frac{Sf1}{K_{Sf1} + Sf1}, \qquad h_{StAR}(StAR) = \frac{StAR}{K_{StAR} + StAR},$$

$$f_{ACORT}(StARp37) = \frac{StARp37}{K_{StARp37} + StARp37}, \qquad f_{pGR}(ACORT) = \frac{ACORT}{K_{ACORT} + ACORT},$$

$$f_{dax1}(SF1, pGR) = \frac{\frac{SF1}{K_{SF1}} + \frac{SF1 \cdot pGR}{K_{SF1} \cdot K_G}}{1 + \frac{SF1}{K_{SF1}} + \frac{SF1 \cdot pGR}{K_{SF1} \cdot K_G}}, \qquad f_{stAR}(SF1, DAX1) = \frac{\frac{SF1}{K_{SF1}}}{1 + \frac{SF1}{K_{SF1}} + \frac{DAX1}{K_D}}.$$

Node	Target	Sign	Effect	References
ACTH	*dax*1	–	Inhibits SF1-dependent activation	[Gummow et al., 2006]
	*Dax*1	∓	Modulates mRNA stability	[Ragazzon et al., 2006]
	*sf*1	+	Promoter activation	[Ragazzon et al., 2006]
	*SF*1	–	Protein stabilisation	[Æsøy et al., 2002]
	stAR	+	pCREB-mediated promoter activation	[Sugawara et al., 1997a]
				[Sugawara et al., 1997b]
				[Zhao et al., 2005]
				[Manna et al., 2009]
	*StARp*37	+	PKA-mediated protein stabilisation	[Arakane et al., 1997]
				[Manna et al., 2009]
	HSL	+	PKA-mediated activation (S563 and S660)	[Manna et al., 2013]
		+	AMPK-mediated activation (S565)	[Watt et al., 2006]
	*mc*2*r*	+	Promoter activation	[Winnay and Hammer, 2006]
	mrap	+	Promoter activation	[Gorrigan et al., 2011]
ACORT	pGR	+	Activation through phosphorylation	- - -
pGR	*dax*1	+	SF1-dependent enhancement of Dax1	[Gummow et al., 2006]
*DAX*1	*stAR*	+/–	Inhibits SF1-dependent activation	[Sugawara et al., 1997a]
				[Sugawara et al., 1997b]
				[Fan et al., 2004]
			Activation at high doses	[Xu et al., 2009]
	*mc*2*r*	+	Promoter activation	[Xu et al., 2009]
	*nur*77	–	Promoter inhibition	[Song et al., 2004]
	*NUR*77	–	Protein inhibition	[Song et al., 2004]
*SF*1	*dax*1	+	Promoter activation	[Gummow et al., 2006]
	stAR/*mc*2*r*	+	Promoter activation	[Babu et al., 2002]
				[Gummow et al., 2006]
				[Winnay and Hammer, 2006]
*StARp*37	*StARp*30/Chol	+	Cholesterol import to mitochondria	[Arakane et al., 1997]
				[Manna et al., 2009]
	HSL-S660/Chol	+	Cholesterol biosynthesis	[Shen et al., 2003]
HSL	S565/S563/S660	+/–	Context-dependent phosphorylation	[Kraemer and Shen, 2002]
				[Watt et al., 2006]

Note: Obvious connections (e.g. transcription, translation, ACORT biosynthesis) are not included in this table.

Table A: *Supporting references for cross-talk connections within the adrenal SRN.*

2 Parameter Estimation

The temporal resolution of our experiments is determined by the timescale of the regulatory processes involved, which was in the order of minutes. We set this as the timescale for our kinetic parameters, so that all parametric units were expressed in terms of molar concentrations (M) and minutes (min). Moreover, even though our model equations are considering a single cell system, we must not forget that our experimental measurements were carried out at the tissue level. This means our model predictions could be extrapolated to the total number of cells in the adrenal cortex, provided that the appropriate cellular and nuclear volumes for the different adrenal cell types are accounted for. Though we couldn't find measurements of these volumes in Sprague Dawley rats, we approximated them from a study of the ultrastructure of Wistar rat adrenal cells, which estimates the cell and nuclear volume of steroidogenic ZF cells as $\sim 3600\,\mu m^3$ and $\sim 260\,\mu m^3$, respectively [Nickerson, 1976]. Thus, to deal with Molar units in a simpler way, we used the nuclear volume $V_{nuc} = 2.6 \times 10^{-13}\,lt$ as it is in this cellular enclosure where gene regulatory reactions take place.

Also, note that the regulatory functions have either sigmoidal or Michaelian shapes and that they're normalised (including the multivariate functions). Hence, the overall flux contribution of these terms is to modulate the weight of kinetic rates (small k's), whereas their sensitivity to activation by the independent variable is represented by the half-maximum constants (big K's), i.e. the concentration at which the i-th factor reaches $\frac{1}{2}$.

In what follows, we estimate the kinetic rates and other parameter values. A comprehensive summary of these values is shown in Table B.

2.1 Basal Transcription Rates

The basal transcription rates, denoted by the σ's, are the rates at which the gene promoters are activated without the influence of any of the above-mentioned transcription regulators (thought other factors may be involved), or the minimum level of transcription that these regulators may exert on the gene (see for instance the influx term in Eq. 7 when ACTH is absent). For the sake of simplicity, we assumed that basal transcription rates amounted to 5% of the maximum transcription rates. That is:

$$\sigma_{dax1} = 0.05 * k_{dax1}, \quad \sigma_{sf1} = 0.05 * k_{sf1}, \quad \sigma_{stAR} = 0.05 * k_{stAR}.$$

2.2 Transcription, Translation and Activation Rates

We calculated the maximum rate of gene expression, assessed by the synthesis of the nascent transcript, as:

$$k_{gene} = \frac{k_{pol}^{max}}{L_{hnRNA} N_A V_{nuc}} D_{gene} \tag{24}$$

where k_{gene} is the maximum transcription rate of the gene, measured in Molar concentration per minute; k_{pol}^{max} is the maximum elongation speed (processivity rate) of the RNA polymerase, measured in number of bases synthesised per gene copy per cell per minute and neglecting pauses in polymerase activity; L_{hnRNA} is the hnRNA transcript length, measured in number of bases per transcript (including introns); N_A is Avogadro's constant; V_{nuc} is the nuclear volume of a Zona Fasciculata (ZF) cell, measured in litres; and D_{gene} is the gene dosage, or number of gene copies within each ZF cell.

The maximum processivity rate of the RNA Pol II in mammalian tissue culture cells is estimated at $71.6\,nt/sec$ [Darzacq et al., 2007], corresponding to a maximum elongation speed of $k_{pol}^{max} \approx 4.3\,kb\,min^{-1}$. Regarding the gene dosage, we only have information for human Dax1 present as a duplicate, with both copies active. Thus, we will assume for all genes that $D_{gene} = 2$. The only parameter that remains undetermined in Eq. 24 is the transcript length, which depends on the gene in question and we calculate below.

For the Dax1 gene, which in rats is known to encode a hnRNA of 4129 b in length [3], we estimate a maximum transcription rate of $k_{dax1} = 1.33 \times 10^{-11}\, M\, min^{-1}$ (after splicing, the mature mRNA is reduced to 1.8 kb in length [4]). Similarly, the SF1 gene in rats is known to encode a hnRNA of 20825 b in length [5], which we estimate will have a maximum transcription rate of $k_{sf1} = 2.64 \times 10^{-12}\, M\, min^{-1}$ (after splicing, the mature mRNA is barely 2182 b in length [6]). Lastly, the StAR gene is known to encode a hnRNA of 4643 b in length [7], for which we estimate a maximum transcription rate of $k_{stAR} = 1.18 \times 10^{-11}\, M\, min^{-1}$ (after splicing, the predominant transcript variant is a 3.5 kb mRNA [Ariyoshi et al., 1998]). Thus:

$$k_{dax1} = 1.33 \times 10^{-11}\, M\, min^{-1}, \quad k_{sf1} = 2.64 \times 10^{-12}\, M\, min^{-1}, \quad k_{stAR} = 1.18 \times 10^{-11}\, M\, min^{-1}.$$

which then implies the basal transcription rates are:

$$\sigma_{dax1} = 6.65 \times 10^{-13}\, M\, min^{-1}, \quad \sigma_{sf1} = 1.32 \times 10^{-13}\, M\, min^{-1}, \quad \sigma_{stAR} = 5.91 \times 10^{-13}\, M\, min^{-1}.$$

The maturation rates of hnRNA into mRNA are likely subject to high variability given the post-processing of transcripts depends on multiple, complex reaction steps (e.g. capping, polyadenylation, splicing, nuclear export) [Keene, 2007]. For the sake of simplicity, we'll assume their values are half the above maximum rates of gene expression. Thus, after halving their values and removing Molar units by multiplying by the product of Avogadro's constant and the nuclear volume, we arrive to:

$$k_{Dax1} = 1.04\, min^{-1}, \quad k_{Sf1} = 0.21\, min^{-1}, \quad k_{StAR} = 0.93\, min^{-1}.$$

We calculate the translation rate (protein synthesis) for any given transcript in a single ZF cell as:

$$k_{protein} = \frac{k_{rib}}{L_{poly}} \tag{25}$$

where $k_{protein}$ is the translation rate of the protein per minute per cell (keeping in mind this rate should be multiplied by the Molar concentration of mRNAs, so that protein concentration changes in units of $M\, min^{-1}$); k_{rib} is the polypeptide elongation speed (processivity rate) of the ribosome, measured in number of codons translated (or aa's synthesised) per transcript per cell per minute and assuming ribosome stalling is already accounted for; and L_{poly} is the polypeptide length, measured in number of aa's (we account for the polypeptide length instead of the mRNA length as UTR regions do not contribute to protein synthesis). We will use the average ribosome progression rate for translation in *Mus musculus* as a proxy for that of rat, which was unavailable. This is estimated at 5.6 ± 0.5 codons per second, which equals to $k_{rib} \approx 336\, aa\, min^{-1}$ [Ingolia et al., 2011].

Considering the rat $DAX1$ polypeptide is 472 aa in length [8], we estimate a translation rate of $k_{DAX1} = 0.71\, min^{-1}$. Similarly, the SF1 polypeptide in rats is 462 aa in length [9], which corresponds to a translation rate of $k_{SF1} = 0.73\, min^{-1}$. Lastly, for the StAR protein precursor (the 37 kDa form $StARp37$), we can assume as a "rule of thumb" a molecular weight of 100-110 Da per average amino acid [Phillips et al., 2009]; assuming the newly synthesised $StARp37$ is $\sim 336\, aa$ in length (the 32 kDa form is 284 aa long [10]), we can estimate a translation rate of $k_{StARp37} = 1\, min^{-1}$. Thus:

$$k_{DAX1} = 0.71\, min^{-1}, \quad k_{SF1} = 0.73\, min^{-1}, \quad k_{StARp37} = 1\, min^{-1}.$$

[3] http://www.ensembl.org/Rattus_norvegicus/Transcript/Exons?db=core;g=ENSRNOG00000003765;r=X:54734385-54738513;t=ENSRNOT00000005023

[4] http://www.ncbi.nlm.nih.gov/nuccore/NM_053317.1

[5] http://www.ensembl.org/Rattus_norvegicus/Transcript/Exons?db=core;g=ENSRNOG00000012682;r=3:22999616-23020441;t=ENSRNOT00000017651

[6] http://www.ncbi.nlm.nih.gov/nuccore/NM_001191099.1

[7] http://www.ensembl.org/Rattus_norvegicus/Transcript/Exons?db=core;g=ENSRNOG00000015052;r=16:71036204-71040847;t=ENSRNOT00000020606

[8] http://www.uniprot.org/uniprot/P70503

[9] http://www.uniprot.org/uniprot/P50569

[10] http://www.uniprot.org/uniprot/P97826

Lastly, we chose the parameters k_{ACORT} and k_{GR} arbitrarily and allow them to vary during our model fitting to data as a means to probe the negative feedback strength. For these values, we assumed

$$k_{ACORT} = 6.39 \times 10^{-12}\, M\, min^{-1}, \quad k_{GR} = 1 \times 10^{-12}\, M\, min^{-1}.$$

where the chosen value for k_{ACORT} is just 1 divided by the product of the nuclear volume and Avogadro's constant.

2.3 Delays

From the HPA model proposed in [Walker et al., 2010], the overall delay for ACTH signal transduction within the adrenal has been estimated to be $\tau_{Adrenal} \in [6.5, 20]\, min$. However, recent detailed experiments suggest two different time scales for the intra-adrenal network responsiveness, one for the slow genomic pathway and another for the fast, non-genomic one. Specifically, an *intra venous* (i.v.) pulse of ACTH produced rapid, transient increases in plasma CORT, with maximal responses achieved after 5 to 15 *min* (though some *in vitro* studies show ACTH can trigger CORT synthesis within $\sim 3\, min$), and a decrease to almost basal levels at $\sim 30\, min$. In contrast, *StAR* and P450scc hnRNA levels increased at $15\, min$ following ACTH and decreased towards basal values after $30\, min$ [Spiga et al., 2011a]. Hence, we can assume $\tau^{Non-genomic}_{Adrenal} \leq 5\, min$ and $\tau^{Genomic}_{Adrenal} \approx 15\, min$.

The case of the StAR gene is of particular interest since it is known to control the limiting step in CORT biosynthesis, which occurs very rapidly during the adrenal response to ACTH stimulation. From [Miller, 2013], we know that on a $15 - 60\, min$ time scale, ACTH rapidly stimulates both the activation of pre-existing StAR protein and its *de novo* the synthesis. ACTH/cAMP doubles the activity of StAR proteins almost immediately [Arakane et al., 1997] and induces transcription of the StAR gene within minutes [Manna et al., 2009]. *StARp*37 then interacts with a complex macromolecular machine in the Outer Mitochondrial Membrane (OMM) that increases the flow of cholesterol from the OMM to the Inner Mitochondrial Membrane (IMM), where it becomes the substrate for CORT biosynthetic enzymes. Thus, we can assume that CORT synthesis is triggered almost instantaneously, whereas StAR gene expression kicks in until a few minutes later.

We can estimate the delays in the genomic pathway by taking into account the gene and hnRNA lengths, together with the processivity rate of the RNA Pol II and the ribosome. The StAR gene, for instance, is known to encode a hnRNA which is $4643\, b$ long. As mentioned before, the maximum processivity rate of the RNA Pol II in mammalian tissue culture cells is estimated at $71.6\, nt/sec = 4.3\, kb/min$ [Darzacq et al., 2007], which means the *StAR* hnRNA would take $\sim 1.08\, min$ to be transcribed. This transcriptional delay would be unusually short, and we should note that additional processes occur during transcript elongation, such as cumulative pauses of $\sim 4\, min$ in average for polymerases on genes. After accounting for stalling effects on a variety of genes, the same study reports an average processivity rate for RNA Pol II as small as $6.3\, nt/sec$. However, we must keep in mind that these measurements are subject to high variability, depending on the gene, the physiological conditions, and the cell type. For instance, in rat kidney cells the reactivation of serum responsive genes following serum deprivation suggests a synthetic rate of 1.1–1.4 kb/min [Femino et al., 1998], whereas a more recent study performed on mouse ES cells determined that the RNA Pol II elongation rates ranged between 0.5 to $4\, kb/min$ [Jonkers et al., 2014]. In summary, several studies where measurements were taken by different techniques and in different conditions place the RNA Pol II elongation speed between 18 and $72\, nt/sec$ [Swinburne and Silver, 2008], with most studies reporting values in the lower half of this range. Here, we will assume an average value of $30\, nt/sec = 1.8\, kb/min$.

Using this average processivity rate, the *stAR* transcriptional delay would be of $2.58\, min$. Regarding transcript editing, we find the duration of an average splicing event has been estimated to last $\sim 30\, sec$ [Hnilicová and Staněk, 2011]. Considering the NCBI reports the StAR gene in *Rattus norvegicus* has 6 introns [11], we can estimate it takes $\sim 3\, min$ for *stAR* hnRNA to mature into *StAR* mRNA, assuming introns are removed sequentially instead of simultaneously and neglecting transcript export to the translation site. Regarding translation, a ribosome progression rate of 5.6 ± 0.5

[11] http://www.ncbi.nlm.nih.gov/gene/25557

codons per second in *Mus musculus* has been reported [Ingolia et al., 2011]. Considering a newly synthesised $StARp37$ precursor protein would have $\sim 336\,aa$ in length (the 32 kDa form is $284\,aa$ long [12]), we can estimate a translation delay of $\sim 1\,min$ assuming a "rule of thumb" of 100-110 Da per average amino acid [Phillips et al., 2009]. Following this, we estimated the delays for StAR gene expression as

$$\tau_{StAR} = 5.58\,min, \quad \tau_{StARp37} = 1\,min.$$

Likewise, the SF1 gene in rats is known to encode a hnRNA which is $20825\,b$ long. Using the same average RNA Pol II processivity rate as before, we estimate it would take $\sim 11.57\,min$ to be transcribed. As the transcript has 6 introns in total [13], we can estimate $\sim 3\,min$ for hnRNA to mature into mRNA, assuming introns are spliced sequentially and not simultaneously. Regarding translation, and considering the rat $SF1$ polypeptide is $462\,aa$ in length [14], we can estimate a translation delay of $\sim 1.38\,min$. Following this, we estimated the delays for the SF1 gene expression as

$$\tau_{Sf1} = 14.57\,min, \quad \tau_{SF1} = 1.38\,min.$$

Lastly, the Dax1 gene in rats is known to encode a hnRNA which is $4129\,b$ long. Using the same average RNA Pol II processivity rate as before, we estimate it would take $\sim 2.29\,min$ to be transcribed. As the transcript has only 1 intron in total [15], we can estimate $\sim 0.5\,min$ for $dax1$ hnRNA to mature into $Dax1$ mRNA. Regarding translation, and considering the rat $DAX1$ polypeptide is $472\,aa$ in length [16], we can estimate a translation delay of $\sim 1.4\,min$. Following this, we estimated the delays for Dax1 gene expression as

$$\tau_{Dax1} = 2.79\,min, \quad \tau_{DAX1} = 1.4\,min.$$

2.4 Degradation Rates

For simplicity, we'll assume that immature, uncapped, non-polyadenylated hnRNAs will have a degradation rate an order of magnitude faster than their mature mRNA counterparts. This results in half-lives for hnRNAs of $\sim 20\,min$, comparable to those estimated previously for primary transcripts in a model of RNA metabolism in mammalian cells [Jackson et al., 2000]. However, after comparing the model predictions with our data, we required to slightly adjust some of our estimations. This likely arises from previously unaccounted context-dependent degradation processes, as we will see in what follows.

$Dax1$ mRNA half-life is reported by [Ragazzon et al., 2006] to be $3\,hrs$. This value corresponds to a degradation rate of $\gamma_{Dax1} = 3.85 \times 10^{-3}\,min^{-1}$. After fitting the model to data regarding the hnRNA half-life and considering a protein half-life of $6\,hrs$ [Osman et al., 2002], we arrive to the following estimates for the Dax1 gene:

$$\gamma_{dax1} = 1.5 \times 10^{-2}\,min^{-1}, \quad \gamma_{Dax1} = 3.85 \times 10^{-3}\,min^{-1}, \quad \gamma_{DAX1} = 1.93 \times 10^{-3}\,min^{-1}.$$

To the best of our knowledge, there is no data available regarding $Sf1$ mRNA stability. Nonetheless, we can assume that, because its mRNA is ~ 400 bases longer than the $Dax1$ transcript, it degrades at a slower rate. Thus, after calculating a longer half-life in proportion to its length as compared to the $Dax1$ transcript, we estimated a degradation rate for the $Sf1$ mRNA of $3.18 \times 10^{-3}\,min^{-1}$. This rate, however, had to be expressed in different units after the model fitting to data suggested that this degradation was better represented through a Michaelis-Menten mechanism. Thus, the $Sf1$ degradation rate was set to $\gamma_{Sf1} = 2.03 \times 10^{-14}\,M\,min^{-1}$. The $sf1$ hnRNA degradation rate, in contrast, was assumed an order of magnitude larger than its mRNA counterpart. In the proper units, this was set as $\gamma_{sf1} = 3.18 \times 10^{-2}\,min^{-1}$. Regarding the $SF1$ protein, previously [Jacob et al., 2001] and [Chen et al., 2007] have estimated its half-life between $2.5 - 4\,hrs$, corresponding to

[12] http://www.uniprot.org/uniprot/P97826
[13] http://www.ncbi.nlm.nih.gov/gene/83826
[14] http://www.uniprot.org/uniprot/P50569
[15] http://www.ncbi.nlm.nih.gov/gene/58850
[16] http://www.uniprot.org/uniprot/P70503

a degradation rate within the range $2.89 \times 10^{-3}\, min^{-1}$ to $4.62 \times 10^{-3}\, min^{-1}$. However, we must take into account the PKA-mediated stabilisation effects of ACTH upon $SF1$. For instance, [Æsøy et al., 2002] found a significant reduction in $SF1$ protein amount in transfected COS-1 cells in the absence of PKA-Cα overexpression measured $4\, hrs$ post chase ($mean \pm SEM = 23.7 \pm 4.64\%$, $P = 0.0022$), compared with the amount of $SF1$ protein after $1\, hr$, which was set to 100%. In contrast, no significant reduction in $SF1$ protein amount was observed after $4\, hrs$ in cells cotransfected with PKA-Cα ($mean \pm SEM = 77.2 \pm 9.5\%$, $P = 0.143$). Thus, it seems that the turnover of transiently expressed $SF1$ was decreased by coexpression of PKA-Cα. Solving the differential equation for first order degradation, we find the degradation rate is given by:

$$\gamma = \frac{1}{t} \ln \frac{x_0}{x(t)} \tag{26}$$

which we can use to calculate $\gamma_{SF1}^{PKA-} = 8 \times 10^{-3}\, min^{-1}$ and $\gamma_{SF1}^{PKA+} = 1.44 \times 10^{-3}\, min^{-1}$. Here, we will use the first value, as by including the function $g_{SF1}^{-}(ACTH)$ in the turnover term in Eq. 11 we account for the PKA-mediated stabilising effects of ACTH stimuli. Thus, for the SF1 gene, in the absence of ACTH stimulation, we will have:

$$\gamma_{sf1} = 3.18 \times 10^{-2}\, min^{-1}, \quad \gamma_{Sf1} = 2.03 \times 10^{-14}\, M\, min^{-1}, \quad \gamma_{SF1} = 8 \times 10^{-3}\, min^{-1}.$$

The available information regarding $StAR$ mRNA stability is a bit controversial, especially since two isoforms have been reported, each with different half-lives and the possibility of selective degradation in steroidogenic cells [Duan and Jefcoate, 2007]. As before, we could make an estimation based on its transcript length being twice as long as the $Dax1$ mRNA. Following this, we estimated a degradation rate of $1.98 \times 10^{-3}\, min^{-1}$. However, at the moment of fitting the model to data from the ACTH i.v. pulse experiment, we found that this degradation rate had to be approximately twice as large. Accordingly, we have modified it to $\gamma_{StAR} = 3.96 \times 10^{-3}\, min^{-1}$. Likewise, the value of the $stAR$ hnRNA degradation was adjusted after fitting the model to data and was fixed at $\gamma_{stAR} = 1 \times 10^{-1}\, min^{-1}$. The increase in the γ_{StAR} degradation rate, when compared to the value we originally estimated for $StAR$ mRNA is also supported by experimental evidence showing this gene contains three conserved AU-rich (AURE) element motifs known to mediate fast mRNA turnover [Zhao et al., 2005; Duan and Jefcoate, 2007]. Moreover, the measured half-life for the $3.5\, kb$ $StAR$ mRNA isoform corresponds to a degradation rate of $3.3 \times 10^{-3}\, min^{-1}$, which is close to our estimated value.

The estimation of the $StARp37$ protein turnover rate requires careful examination. According to [Arakane et al., 1997], the StAR protein has a short half-life, but a specific value is not reported. The half-life reported by [Ragazzon et al., 2006] is $\sim 5\, hrs$, with the primary source being [Granot et al., 2003]. However, this value refers to mitochondrial $30\, kDa$ $StAR$, which lacks the N-terminus mitochondrial targeting sequence and it's not involved in cholesterol import into mitochondria. This sequence is cleaved upon the $StAR$ $37\, kDa$ import into mitochondria, a process that influences the rate of the $StARp37$ precursor cytosolic proteasome degradation, according to [Granot et al., 2003].

Both [Arakane et al., 1998] and [Granot et al., 2003] estimate that the $StARp37$ precursor has a half-life of $\sim 15\, min$. However, this estimate accounts only for proteasome-assisted degradation, and the authors suggest that a fast import of the precursor into mitochondria would decrease the time it remains active. This would effectively increase the precursor's lability when both degradation and translocation processes are accounted for, thus decreasing the half-life to $\leq 5\, min$ [Manna et al., 2009; Clark and Hudson, 2015]. This is consistent with previous estimations of $StARp37$ exhibiting a half-life of $5\, min$ in mouse Y1 cells [Artemenko et al., 2001], and of $3 - 4\, min$ in rat adrenal cells incubated at 37 ℃ [Epstein and Orme-Johnson, 1991].

How then is it possible for adrenal cells to exhibit such a fast steroidogenic response while depending upon a precursor protein that is so labile? As it turns out, PKA-mediated ACTH stimulation induces rapid phosphorylation of the precursor $StARp37$, thus stabilising it in the cytosol and enhancing its activity. In other words, ACTH stimulation increases the residence time of $StARp37$ in the cytosol, thus increasing the rate of cholesterol import into mitochondria and enabling the fast response of the adrenal to synthesise CORT.

In summary, we have that when mitochondrial import is blocked, the half-life of the StAR precursor is $15\,min$, corresponding to $\gamma_{StARp37} = 4.62 \times 10^{-2}\,min^{-1}$; but when both mechanisms are blocked the precursor accumulates in the cytosol and its half-life increases up to $6.5\,hrs$, corresponding to a much lower turnover rate of $\mu_{StARp37} = \cancel{\gamma_{StARp37}} + \cancel{\epsilon_{StARp37}} = 1.78 \times 10^{-3}\,min^{-1}$ [Granot et al., 2003]. In contrast, when both protein degradation and mitochondrial import are fully functional, and in the absence of ACTH stimulation, the protein is extremely labile, with a half-life of $\sim 3.5\,min$, corresponding to $\mu^{ACTH-}_{StARp37} = \gamma_{StARp37} + \epsilon_{StARp37} = 1.98 \times 10^{-1}\,min^{-1}$ [Epstein and Orme-Johnson, 1991]. However, upon PKA-mediated phosphorylation of the precursor after ACTH stimulation, the $StARp37$ stabilises and its effective turnover rate drops by two orders of magnitude down to $\mu^{ACTH+}_{StARp37} = \gamma_{StARp37} + \epsilon_{StARp37} = 1.49 \times 10^{-3}\,min^{-1}$ [Clark and Hudson, 2015]. Thus

$$\mu^{ACTH-}_{StARp37} = 1.98 \times 10^{-1}\,min^{-1}$$
$$\mu^{ACTH+}_{StARp37} = 1.49 \times 10^{-3}\,min^{-1}$$

The transition from a very high to a very low turnover rate for $StARp37$ is represented in the second term in Eq. 18 by introducing the function $g^{-}_{StARp37}(ACTH)$ (Eq. 19), which modulates the removal rate $\mu_{StARp37}$. As the decrease in the turnover rate upon ACTH stimulation is quite large, we can fix the parameter as $\mu_{StARp37} = 1.98 \times 10^{-1}\,min^{-1}$ when no ACTH stimulation is present and let the function $g^{-}_{StARp37}(ACTH)$ stabilise $StARp37$. Summarising for the StAR gene, the turnover rates are:

$$\gamma_{stAR} = 1 \times 10^{-1}\,min^{-1}, \quad \gamma_{StAR} = 3.96 \times 10^{-3}\,min^{-1}, \quad \gamma_{StARp37} = 1.98 \times 10^{-1}\,min^{-1}.$$

Though the half-life of intra-adrenal corticosterone ($ACORT$) has not been measured directly, given its rapid export to the bloodstream we can assume it has a faster removal rate than its plasma counterpart. Assuming a half-life of $1\,min$, we estimate a turnover rate of

$$\mu_{ACORT} = 6.93 \times 10^{-1}\,min^{-1}$$

Lastly, for the phosphorylated glucocorticoid receptor (pGR), we find from [Bodwell et al., 1998] that the mouse GR is very stable, with a half-life of $\sim 18\,hrs$ (reduced down to $8 - 9\,hrs$ upon dexamethasone stimulation). However, we're interested in the half-life of the active, phosphorylated form of GR. This is likely to be much more short-lived, but nonetheless has not been measured. For the sake of simplicity, we assume it's half-life is the same as that of $ACORT$, which implies a turnover rate of

$$\gamma_{pGR} = 6.93 \times 10^{-1}\,min^{-1}$$

2.5 Half-Maximum Constants

The half-maximum constants (big K's) are arbitrary parameters that nonetheless capture the sensitivity of a process (e.g. synthesis or degradation) affecting the dynamics of a molecular species Y as a function of the concentration of another species X. As the molecular mechanisms underlying these processes are often unknown, we model them as Michaelis-Menten and Hill type functions. In the latter case, when the Hill coefficient is high enough, these K's could also be interpreted as activation thresholds. Though arbitrary, their relative values are informative of how sensitive different nodes within the adrenal SRN are to common external *stimuli* (e.g. ACTH and cytokines).

Half-maximum constants were estimated manually after observing the system's time evolution and correcting our model for the timescales at which the peak of the transient response, together with the rising and decreasing phases, followed the experimental data. The estimated K's are listed in Table B and represented graphically in Fig. S9. The half-maximum constants that are neither dependent on ACTH nor cytokines, but are rather involved in $Dax1$, $Sf1$ and $StAR$ mRNA degradation, in $ACORT$ and pGR synthesis, and in regulation of Dax1 and StAR gene promoters, were also fixed manually to values close to the range observed during their circadian dynamics.

Of particular interest are the constants $K^{ACTH-lo}_{Dax1}$ and $K^{ACTH-hi}_{Dax1}$ which, respectively, represent the lower and upper *near* half-maximum constants for a non-monotonous regulatory function (Eq. 5)

that models dose-dependent effects of ACTH upon *Dax*1 mRNA stability (Fig. S4). We hypothesise that this dose-dependent degradation of *Dax*1 mRNA could be a post-transcriptional regulatory mechanism such as stress-induced non-sense mediated mRNA decay [He and Jacobson, 2015].

Basal Transcription Rates		
$\sigma_{dax1} = 6.65 \times 10^{-13}\, M\, min^{-1}$	$\sigma_{sf1} = 1.32 \times 10^{-13}\, M\, min^{-1}$	$\sigma_{stAR} = 5.91 \times 10^{-13}\, M\, min^{-1}$
Transcription, Translation and Activation Rates		
$k_{dax1} = 1.33 \times 10^{-11}\, M\, min^{-1}$	$k_{sf1} = 2.64 \times 10^{-12}\, M\, min^{-1}$	$k_{stAR} = 1.18 \times 10^{-11}\, M\, min^{-1}$
$k_{Dax1} = 1.04\, min^{-1}$	$k_{Sf1} = 0.21\, min^{-1}$	$k_{StAR} = 0.93\, min^{-1}$
$k_{DAX1} = 0.71\, min^{-1}$	$k_{SF1} = 0.73\, min^{-1}$	$k_{StARp37} = 1\, min^{-1}$
$k_{ACORT} = 6.39 \times 10^{-12}\, M\, min^{-1}$	$k_{GR} = 1 \times 10^{-12}\, M\, min^{-1}$	
Degradation Rates		
$\gamma_{dax1} = 1.5 \times 10^{-2}\, min^{-1}$	$\gamma_{sf1} = 3.18 \times 10^{-2}\, min^{-1}$	$\gamma_{stAR} = 1 \times 10^{-1}\, min^{-1}$
$\gamma_{Dax1} = 3.85 \times 10^{-3}\, min^{-1}$	$\gamma_{Sf1} = 2.03 \times 10^{-14}\, M\, min^{-1}$	$\gamma_{StAR} = 3.96 \times 10^{-3}\, min^{-1}$
$\gamma_{DAX1} = 1.93 \times 10^{-3}\, min^{-1}$	$\gamma_{SF1} = 8 \times 10^{-3}\, min^{-1}$	$\mu_{StARp37} = 1.98 \times 10^{-1}\, min^{-1}$
$\mu_{ACORT} = 6.93 \times 10^{-1}\, min^{-1}$	$\gamma_{pGR} = 6.93 \times 10^{-1}\, min^{-1}$	
Delays		
$\tau_{Dax1} = 2.79\, min$	$\tau_{Sf1} = 14.57\, min$	$\tau_{StAR} = 5.58\, min$
$\tau_{DAX1} = 1.4\, min$	$\tau_{SF1} = 1.38\, min$	$\tau_{StARp37} = 1\, min$
Half-Maximum Constants		
$K_{dax1}^{ACTH} = 90\, pg\, ml^{-1}$	$K_{ACORT} = 4.5\, AU$	$K_{dax1}^{IL6} = K_{Dax1}^{IL6} = K_{DAX1}^{IL6} = 500\, AU$
$K_{Dax1}^{ACTH-lo} = 30\, pg\, ml^{-1}$	$K_G = 0.76\, AU$	$K_{sf1}^{IL6} = 1000\, AU$
$K_{Dax1}^{ACTH-hi} = 1000\, pg\, ml^{-1}$	$K_D = 5.7 \times 10^{-5}\, M$	$K_{Sf1}^{IL6} = K_{SF1}^{IL6} = 100\, AU$
$K_{sf1}^{ACTH} = 30\, pg\, ml^{-1}$	$K_{Sf1} = 1 \times 10^{-8}\, M$	$K_{StAR}^{IL6} = 2500\, AU$
$K_{SF1}^{ACTH} = 70\, pg\, ml^{-1}$	$K_{SF1} = 6.2 \times 10^{-7}\, M$	$K_{StARp37}^{IL6} = 500\, AU$
$K_{stAR}^{ACTH} = 70\, pg\, ml^{-1}$	$K_{StAR} = 1 \times 10^{-8}\, M$	$K_{stAR}^{IL1\beta} = 200\, AU$
$K_{StARp37}^{ACTH} = 70\, pg\, ml^{-1}$	$K_{StARp37} = 4 \times 10^{-8}\, M$	$K_{stAR}^{TNF\alpha} = K_{StAR}^{TNF\alpha} = 60\, AU$
		$K_{pGR}^{TNF\alpha} = 20\, AU$

Table B: *Kinetic rates and other estimated parameter values.*

3 Crosstalk Between the Adrenal SRN and the Immune Pathway

Stimulation of rats with the bacterial lipopolysaccharide (LPS) endotoxin elicits a strong response not only at the HPA level but also on the immune system. In particular, LPS induces cytokines $TNF\alpha$, $IL1\beta$ and $IL6$[17], which are known to act upon targets of the adrenal SRN and among themselves.

A previous mathematical model by [Malek et al., 2015] suggested a way in which LPS, $TNF\alpha$ and $IL6$ may interact with ACTH and CORT to mediate the adrenal response to inflammation. However, such a model assumed direct interactions of these cytokines upon ACTH, ignoring the steroidogenic pathway within adrenal cells. LPS effects on the immune system are more complex and start with the recruitment of macrophages to the adrenal cortex. This increases levels of $TNF\alpha$ in a first stage (peak at $60\,min$), and of $IL1\beta$ and $IL6$ (in T-lymphocytes) in a second stage (peaks at $120\,min$) [Givalois et al., 1994]. While it is believed that the first stage is amplified through a positive feedback, in the second one $IL1\beta$ and $IL6$ are known to inhibit rising levels of $TNF\alpha$. Moreover, though CORT is known to inhibit both $IL1\beta$ and $IL6$, it has been proposed that $IL1\beta$ is involved in the initial activation of CORT production, whereas $IL6$ sustains it [Givalois et al., 1994; Kanczkowski et al., 2013]. These interactions between LPS and cytokines, together with the crosstalk between the immune pathway and the adrenal SRN (Table C), is summarised in Fig. S8.

Even though the interactions among cytokines are complex, we know that the output of the internal crosstalk within the immune pathway upon an LPS challenge delivers the measured levels of $TNF\alpha$, $IL1\beta$ and $IL6$ (Fig. S7a-c). Thus, we can ignore the interactions within the immune pathway as long as we account for the effects of cytokines upon specific targets of the adrenal SRN. This effectively means that, during an LPS challenge, in addition to an ACTH input we will now use the time course of these cytokines as input functions. The task becomes complex as soon as we realise that the experimental evidence available comes from different cell types and animal models (Table C).

3.1 Model Equations for the SRN with Cytokine Interactions

We explored different network architectures and arrived to the scenario depicted in Fig. 5, which is associated to the following set of model equations, where the cytokine effects are shown in red:

$$
\begin{aligned}
\dot{dax1} &= \sigma_{dax1} + k_{dax1} f_{dax1}(SF1, pGR) g^{-}_{dax1}(ACTH) \phi_{dax1}(IL6) - \gamma_{dax1} dax1, \\
\dot{Dax1} &= k_{Dax1} dax1_{\tau_{Dax1}} \phi_{Dax1}(IL6) - \gamma_{Dax1} Dax1 g^{\mp}_{Dax1}(ACTH), \\
\dot{DAX1} &= k_{DAX1} Dax1_{\tau_{DAX1}} \phi_{DAX1}(IL6) - \gamma_{DAX1} DAX1, \\
\dot{sf1} &= \sigma_{sf1} + k_{sf1} g^{+}_{sf1}(ACTH) \phi_{sf1}(IL6) - \gamma_{sf1} sf1, \\
\dot{Sf1} &= k_{Sf1} sf1_{\tau_{Sf1}} \phi_{Sf1}(IL6) - \gamma_{Sf1} h_{Sf1}(Sf1), \\
\dot{SF1} &= k_{SF1} Sf1_{\tau_{SF1}} \phi_{SF1}(IL6) - \gamma_{SF1} SF1 g^{-}_{SF1}(ACTH), \\
\dot{stAR} &= \sigma_{stAR} + k_{stAR} f_{stAR}(SF1, DAX1) g^{+}_{stAR}(ACTH) \phi_{stAR}(TNF\alpha) \phi_{stAR}(IL1\beta) - \gamma_{stAR} stAR, \\
\dot{StAR} &= k_{StAR} stAR_{\tau_{StAR}} \phi_{StAR}(TNF\alpha) \phi_{StAR}(IL6) - \gamma_{StAR} h_{StAR}(StAR), \\
\dot{StARp37} &= k_{StARp37} StAR_{\tau_{StARp37}} \phi_{StARp37}(IL6) - \mu_{StARp37} StARp37 g^{-}_{StARp37}(ACTH), \\
\dot{ACORT} &= k_{ACORT} f_{ACORT}(StARp37) - \mu_{ACORT} ACORT, \\
\dot{pGR} &= k_{GR} f_{pGR}(ACORT) \phi_{pGR}(TNF\alpha) - \gamma_{pGR} pGR.
\end{aligned}
$$

[17] The hyphen in *TNF-α*, *IL-1β*, and *IL-6* labels was dropped to avoid confusion with a minus sign.

where

$$\phi_{dax1}(IL6) = \frac{K_{dax1}^{IL6}}{K_{dax1}^{IL6} + IL6}, \qquad \phi_{stAR}(TNF\alpha) = 1 + \frac{TNF\alpha}{K_{stAR}^{TNF\alpha} + TNF\alpha},$$

$$\phi_{Dax1}(IL6) = \frac{K_{Dax1}^{IL6}}{K_{Dax1}^{IL6} + IL6}, \qquad \phi_{stAR}(IL1\beta) = 1 + \frac{IL1\beta}{K_{stAR}^{IL1\beta} + IL1\beta},$$

$$\phi_{DAX1}(IL6) = \frac{K_{DAX1}^{IL6}}{K_{DAX1}^{IL6} + IL6}, \qquad \phi_{StAR}(TNF\alpha) = 1 + \frac{TNF\alpha}{K_{StAR}^{TNF\alpha} + TNF\alpha},$$

$$\phi_{sf1}(IL6) = \frac{K_{sf1}^{IL6^4}}{K_{sf1}^{IL6^4} + IL6^4}, \qquad \phi_{StAR}(IL6) = \frac{K_{StAR}^{IL6}}{K_{StAR}^{IL6} + IL6},$$

$$\phi_{Sf1}(IL6) = \frac{K_{Sf1}^{IL6^4}}{K_{Sf1}^{IL6^4} + IL6^4}, \qquad \phi_{StARp37}(IL6) = \frac{K_{StARp37}^{IL6}}{K_{StARp37}^{IL6} + IL6},$$

$$\phi_{SF1}(IL6) = \frac{K_{SF1}^{IL6}}{K_{SF1}^{IL6} + IL6}, \qquad \phi_{pGR}(TNF\alpha) = \frac{K_{pGR}^{TNF\alpha}}{K_{pGR}^{TNF\alpha} + TNF\alpha}.$$

As before, the half-maximum constants for the cytokine effects upon targets of the adrenal SRN can be understood as sensitivities. These were estimated by manually fitting the model predictions to experimental data from the LPS challenge experiments. The values are listed in Table B and represented graphically in Fig. S9d-f.

Cytokine	Target	Sign	Cell type/species	Reference
$TNF\alpha$	StAR mRNA/protein	–	Rat testis Leydig tumor cells (LC-540)	[Sadasivam et al., 2015]
	StAR mRNA/protein	–	Mouse macrophage cell line (RAW264.7)	[Ma et al., 2007]
	DAX1 protein	+	Rat testis Leydig tumor cells (LC-540)	[Sadasivam et al., 2015]
	StAR mRNA	+	Human adrenocortical cells (NCI-H295R)	[Tkachenko et al., 2011]
	Cortisol	–	Bovine Zone Fasciculata cells	[Barney et al., 2000]
	pGR	–	Human Airway Smooth Muscle cells	[Bouazza et al., 2012]
$IL1\beta$	StAR mRNA	+	Human adrenocortical cells (NCI-H295R)	[Tkachenko et al., 2011]
$IL6$	StAR mRNA/protein	+	Bovine Zona Fasciculata cells	[McIlmoil et al., 2016]
	Dax1 mRNA/protein	–	Bovine Zona Fasciculata cells	[McIlmoil et al., 2016]
	SF1 mRNA/protein	+	Bovine Zona Fasciculata cells	[McIlmoil et al., 2016]
	StAR mRNA/protein	–	Bovine Zona Reticularis cells	[McIlmoil et al., 2015]
	Dax1 mRNA/protein	+	Bovine Zona Reticularis cells	[McIlmoil et al., 2015]
	SF1 mRNA/protein	–	Bovine Zona Reticularis cells	[McIlmoil et al., 2015]
	StAR mRNA	+	Human adrenocortical cells (NCI-H295R)	[Tkachenko et al., 2011]
	Cortisol	+	Bovine Zona Fasciculata cells	[Barney et al., 2000]
LPS	StAR 30 kDa	–	Rat testis Leydig cells	[Allen et al., 2004]
				[Held Hales et al., 2000]
	StAR 30 kDa	+	Rat adrenal cells	[Held Hales et al., 2000]
	StAR 37 kDa	+	Rat testis Leydig tumor cells	[Allen et al., 2004]
	StAR	+	Mouse Y1 cells	[Calejman et al., 2011]
	Corticosterone	+	Rat adrenal cells	[Calejman et al., 2011]

Table C: *Cytokine effects upon targets within the adrenal SRN.*

3.2 Scaling Model Outputs of Cytokine Targets

Even though our model predicts the time evolution of hnRNA, mRNA, and protein concentrations, these predictions are inherently qualitative. This is mainly because we have approximated the mechanisms underlying gene regulation through Hill type functions and, to a lesser degree, because our model doesn't account for regulatory processes affecting mRNA and protein stability.

However, in order to make our model predictions comparable to the experimental data (expressed in $pg/\mu g$ for ACORT and as fold induction for all other variables), we have implemented a variable change to express the model predictions in terms of dimensionless arbitrary units. To do this consistently, all x state variables in the model were transformed according to the formula:

$$\hat{x} = \frac{x - x_{t=0}}{x_{max} - x_{min}}\sigma_x + offset$$

where $x_{t=0}$ is the value of x at the time the pulse is given, x_{max} and x_{min} are the maximum and minimum value of the response, and σ_x is a scaling factor. The *offset* value was set to 1 for all state variables with data reported as fold induction, except for ACORT, which experiments reported as $pg/\mu g$ and for which we set an *offset* of 25, following the baseline observed in ACTH i.v. pulse experiments.

The scaling factors were adjusted to reproduce the data of the ACTH i.v. pulse experiment, and these remained invariant when the model was used to predict the high s.c. ACTH pulse and LPS challenge data without cytokines (Table D). The only scenario where scaling factors were allowed to vary was after modifying the existing model to account for cytokine effects. Interestingly, in this latter case most scaling factors remain invariant, except for those multiplying variables targeted by cytokines. As before, this is because we have used Hill type functions to approximate the mechanisms by which these pro-inflammatory cytokines interact with targets of the SRN.

Variable	**ACTH small i.v. pulse**	**ACTH high s.c. pulse**	**LPS challenge without cytokines**	**LPS challenge with cytokines**
ACORT	300	300	300	300
pGR	3.5	3.5	3.5	0.4
dax1 hnRNA	0.9	0.9	0.9	0.9
Dax1 mRNA	0.4	0.4	0.4	0.8
DAX1 protein	0.1	0.1	0.1	0.6
sf1 hnRNA	0.6	0.6	0.6	0.6
Sf1 mRNA	0.5	0.5	0.5	0.1
SF1 protein	0.2	0.2	0.2	0.2
stAR hnRNA	3	3	3	3
StAR mRNA	2	2	2	2
StARp37 protein	0.1	0.1	0.1	2

Table D: *Scaling factors σ_x. Values in red correspond to non-statistically significant data. All scaling factors remain invariant in the model, except when the model is modified to account for cytokine inputs (last column) and only on molecular species targeted by cytokines (Fig. 5).*

References

Allen, J. A., Diemer, T., Janus, P., Hales, K. H., and Hales, D. B. (2004). Bacterial endotoxin lipopolysaccharide and reactive oxygen species inhibit leydig cell steroidogenesis via perturbation of mitochondria. *Endocrine*, 25(3):265–275.

Arakane, F., Kallen, C. B., Watari, H., Foster, J. A., Sepuri, N. B. V., Pain, D., Stayrook, S. E., Lewis, M., Gerton, G. L., and Strauss, J. F. (1998). The mechanism of action of steroidogenic acute regulatory protein (star) star acts on the outside of mitochondria to stimulate steroidogenesis. *Journal of Biological Chemistry*, 273(26):16339–16345.

Arakane, F., King, S. R., Du, Y., Kallen, C. B., Walsh, L. P., Watari, H., Stocco, D. M., and Strauss, J. F. (1997). Phosphorylation of steroidogenic acute regulatory protein (star) modulates its steroidogenic activity. *Journal of Biological Chemistry*, 272(51):32656–32662.

Ariyoshi, N., Kim, Y.-C., Artemenko, I., Bhattacharyya, K. K., and Jefcoate, C. R. (1998). Characterization of the rat star gene that encodes the predominant 3.5-kilobase pair mrna acth stimulation of adrenal steroids in vivo precedes elevation of star mrna and protein. *Journal of Biological Chemistry*, 273(13):7610–7619.

Artemenko, I. P., Zhao, D., Hales, D. B., Hales, K. H., and Jefcoate, C. R. (2001). Mitochondrial processing of newly synthesized steroidogenic acute regulatory protein (star), but not total star, mediates cholesterol transfer to cytochrome p450 side chain cleavage enzyme in adrenal cells. *Journal of Biological Chemistry*, 276(49):46583–46596.

Babu, P. S., Bavers, D. L., Beuschlein, F., Shah, S., Jeffs, B., Jameson, J. L., and Hammer, G. D. (2002). Interaction between dax-1 and steroidogenic factor-1 in vivo: increased adrenal responsiveness to acth in the absence of dax-1. *Endocrinology*, 143(2):665–673.

Barney, M., Call, G. B., McIlmoil, C. J., Husein, O. F., Adams, A., Balls, A. G., Oliveira, G. K., Miner, E. C., Richards, T. A., Crawford, B. K., et al. (2000). Stimulation by interleukin-6 and inhibition by tumor necrosis factor of cortisol release from bovine adrenal zona fasciculata cells through their receptors. *Endocrine*, 13(3):369–377.

Bodwell, J. E., Webster, J. C., Jewell, C. M., Cidlowski, J. A., Hu, J.-M., and Munck, A. (1998). Glucocorticoid receptor phosphorylation: overview, function and cell cycle-dependence. *The Journal of steroid biochemistry and molecular biology*, 65(1):91–99.

Bose, H. S., Lingappa, V. R., and Miller, W. L. (2002). Rapid regulation of steroidogenesis by mitochondrial protein import. *Nature*, 417(6884):87–91.

Bouazza, B., Krytska, K., Debba-Pavard, M., Amrani, Y., Honkanen, R. E., Tran, J., and Tliba, O. (2012). Cytokines alter glucocorticoid receptor phosphorylation in airway cells: role of phosphatases. *American journal of respiratory cell and molecular biology*, 47(4):464–473.

Calejman, C. M., Astort, F., Di Gruccio, J., Repetto, E., Mercau, M., Giordanino, E., Sanchez, R., Pignataro, O., Arias, P., and Cymeryng, C. (2011). Lipopolysaccharide stimulates adrenal steroidogenesis in rodent cells by a nfκb-dependent mechanism involving cox-2 activation. *Molecular and cellular endocrinology*, 337(1):1–6.

Chen, W.-Y., Weng, J.-H., Huang, C.-C., and Chung, B.-c. (2007). Histone deacetylase inhibitors reduce steroidogenesis through scf-mediated ubiquitination and degradation of steroidogenic factor 1 (nr5a1). *Molecular and cellular biology*, 27(20):7284–7290.

Clark, B. J. and Hudson, E. A. (2015). Star protein stability in y1 and kin-8 mouse adrenocortical cells. *Biology*, 4(1):200–215.

Darzacq, X., Shav-Tal, Y., de Turris, V., Brody, Y., Shenoy, S. M., Phair, R. D., and Singer, R. H. (2007). In vivo dynamics of rna polymerase ii transcription. *Nature structural molecular biology*, 14(9):796–806.

Duan, H. and Jefcoate, C. R. (2007). The predominant camp-stimulated 3.5 kb star mrna contains specific sequence elements in the extended 3 utr that confer high basal instability. *Journal of molecular endocrinology*, 38(1):159–179.

Epstein, L. and Orme-Johnson, N. (1991). Regulation of steroid hormone biosynthesis. identification of precursors of a phosphoprotein targeted to the mitochondrion in stimulated rat adrenal cortex cells. *Journal of Biological Chemistry*, 266(29):19739–19745.

Ermentrout, B. (2002). *Simulating, analyzing, and animating dynamical systems: a guide to XPPAUT for researchers and students*, volume 14. Siam.

Fan, W., Yanase, T., Wu, Y., Kawate, H., Saitoh, M., Oba, K., Nomura, M., Okabe, T., Goto, K., and Yanagisawa, J. (2004). Protein kinase a potentiates adrenal 4 binding protein/steroidogenic factor 1 transactivation by reintegrating the subcellular dynamic interactions of the nuclear receptor with its cofactors, general control nonderepressed-5/transformation/transcription domain-associated protein, and suppressor, dosage-sensitive sex reversal-1: a laser confocal imaging study in living kgn cells. *Molecular Endocrinology*, 18(1):127–141.

Femino, A. M., Fay, F. S., Fogarty, K., and Singer, R. H. (1998). Visualization of single rna transcripts in situ. *Science*, 280(5363):585–590.

Givalois, L., Dornand, J., Mekaouche, M., Solier, M., Bristow, A., Ixart, G., Siaud, P., Assenmacher, I., and Barbanel, G. (1994). Temporal cascade of plasma level surges in acth, corticosterone, and cytokines in endotoxin-challenged rats. *American Journal of Physiology-Regulatory, Integrative and Comparative Physiology*, 267(1):R164–R170.

Gorrigan, R. J., Guasti, L., King, P., Clark, A. J., and Chan, L. F. (2011). Localisation of the melanocortin-2-receptor and its accessory proteins in the developing and adult adrenal gland. *Journal of molecular endocrinology*, 46(3):227–232.

Granot, Z., Geiss-Friedlander, R., Melamed-Book, N., Eimerl, S., Timberg, R., Weiss, A. M., Hales, K. H., Hales, D. B., Stocco, D. M., and Orly, J. (2003). Proteolysis of normal and mutated steroidogenic acute regulatory proteins in the mitochondria: the fate of unwanted proteins. *Molecular Endocrinology*, 17(12):2461–2476.

Gummow, B. M., Scheys, J. O., Cancelli, V. R., and Hammer, G. D. (2006). Reciprocal regulation of a glucocorticoid receptor-steroidogenic factor-1 transcription complex on the dax-1 promoter by glucocorticoids and adrenocorticotropic hormone in the adrenal cortex. *Mol Endocrinol*, 20(11):2711–23.

He, F. and Jacobson, A. (2015). Nonsense-mediated mrna decay: degradation of defective transcripts is only part of the story. *Annual review of genetics*, 49:339–366.

Held Hales, K., Diemer, T., Ginde, S., Shankar, B. K., Roberts, M., Bosmann, H. B., and Hales, D. B. (2000). Diametric effects of bacterial endotoxin lipopolysaccharide on adrenal and leydig cell steroidogenic acute regulatory protein. *Endocrinology*, 141(11):4000–4012.

Hnilicová, J. and Staněk, D. (2011). Where splicing joins chromatin. *Nucleus*, 2(3):182–188.

Ingolia, N. T., Lareau, L. F., and Weissman, J. S. (2011). Ribosome profiling of mouse embryonic stem cells reveals the complexity and dynamics of mammalian proteomes. *Cell*, 147(4):789–802.

Iyer, A. K., Zhang, Y.-H., and McCabe, E. R. (2007). Lxxll motifs and af-2 domain mediate shp (nr0b2) homodimerization and dax1 (nr0b1)–dax1a heterodimerization. *Molecular genetics and metabolism*, 92(1):151–159.

Jackson, D. A., Pombo, A., and Iborra, F. (2000). The balance sheet for transcription: an analysis of nuclear rna metabolism in mammalian cells. *The FASEB Journal*, 14(2):242–254.

Jacob, A. L., Lund, J., Martinez, P., and Hedin, L. (2001). Acetylation of steroidogenic factor 1 protein regulates its transcriptional activity and recruits the coactivator gcn5. *Journal of Biological Chemistry*, 276(40):37659–37664.

Jasper, M. and Engeland, W. (1994). Splanchnic neural activity modulates ultradian and circadian rhythms in adrenocortical secretion in awake rats. *Neuroendocrinology*, 59(2):97–109.

Jonkers, I., Kwak, H., and Lis, J. T. (2014). Genome-wide dynamics of pol ii elongation and its interplay with promoter proximal pausing, chromatin, and exons. *Elife*, 3:e02407.

Kanczkowski, W., Chatzigeorgiou, A., Samus, M., Tran, N., Zacharowski, K., Chavakis, T., and Bornstein, S. R. (2013). Characterization of the lps-induced inflammation of the adrenal gland in mice. *Molecular and cellular endocrinology*, 371(1):228–235.

Keene, J. D. (2007). Rna regulons: coordination of post-transcriptional events. *Nature Reviews Genetics*, 8(7):533–543.

Kitay, J. I. (1961). Sex differences in adrenal cortical secretion in the rat 1. *Endocrinology*, 68(5):818–824.

Kraemer, F. B. and Shen, W.-J. (2002). Hormone-sensitive lipase control of intracellular tri-(di-) acylglycerol and cholesteryl ester hydrolysis. *Journal of lipid research*, 43(10):1585–1594.

Ma, Y., Ren, S., Pandak, W., Li, X., Ning, Y., Lu, C., Zhao, F., and Yin, L. (2007). The effects of inflammatory cytokines on steroidogenic acute regulatory protein expression in macrophages. *Inflammation research*, 56(12):495–501.

Malek, H., Ebadzadeh, M. M., Safabakhsh, R., Razavi, A., and Zaringhalam, J. (2015). Dynamics of the hpa axis and inflammatory cytokines: Insights from mathematical modeling. *Computers in biology and medicine*, 67:1–12.

Manna, P. R., Cohen-Tannoudji, J., Counis, R., Garner, C. W., Huhtaniemi, I., Kraemer, F. B., and Stocco, D. M. (2013). Mechanisms of action of hormone-sensitive lipase in mouse leydig cells its role in the regulation of the steroidogenic acute regulatory protein. *Journal of Biological Chemistry*, 288(12):8505–8518.

Manna, P. R., Dyson, M. T., and Stocco, D. M. (2009). Regulation of the steroidogenic acute regulatory protein gene expression: present and future perspectives. *Mol Hum Reprod*, 15(6):321–33.

Manna, P. R., Wang, X.-J., and Stocco, D. M. (2003). Involvement of multiple transcription factors in the regulation of steroidogenic acute regulatory protein gene expression. *Steroids*, 68(14):1125–1134.

McIlmoil, S., Call, G., Barney, M., Strickland, J., and Judd, A. (2015). Interleukin-6 inhibits adrenal androgen release from bovine adrenal zona reticularis cells by inhibiting the expression of steroidogenic proteins. *Domestic animal endocrinology*, 53:108–123.

McIlmoil, S., Strickland, J., and Judd, A. (2016). Interleukin 6 increases the in vitro expression of key proteins associated with steroidogenesis in the bovine adrenal zona fasciculata. *Domestic animal endocrinology*, 55:11–24.

Miller, W. L. (2013). Steroid hormone synthesis in mitochondria. *Molecular and cellular endocrinology*, 379(1):62–73.

Niakan, K. and McCabe, E. (2005). Dax1 origin, function, and novel role. *Molecular genetics and metabolism*, 86(1):70–83.

Nickerson, P. (1976). The adrenal cortex in spontaneously hypertensive rats. a quantitative ultrastructural study. *The American journal of pathology*, 84(3):545.

Osman, H., Murigande, C., Nadakal, A., and Capponi, A. M. (2002). Repression of dax-1 and induction of sf-1 expression two mechanisms contributing to the activation of aldosterone biosynthesis in adrenal glomerulosa cells. *Journal of Biological Chemistry*, 277(43):41259–41267.

Phillips, R., Kondev, J., and Theriot, J. (2009). Physical biology of the cell; garland science: New york, 2009.

Ragazzon, B., Lefrançois-Martinez, A.-M., Val, P., Sahut-Barnola, I., Tournaire, C., Chambon, C., Gachancard-Bouya, J.-L., Begue, R.-J., Veyssière, G., and Martinez, A. (2006). Adrenocorticotropin-dependent changes in sf-1/dax-1 ratio influence steroidogenic genes expression in a novel model of glucocorticoid-producing adrenocortical cell lines derived from targeted tumorigenesis. *Endocrinology*, 147(4):1805–1818.

Rankin, J., Walker, J. J., Windle, R., Lightman, S. L., and Terry, J. R. (2012). Characterizing dynamic interactions between ultradian glucocorticoid rhythmicity and acute stress using the phase response curve.

Reul, J. and Kloet, E. D. (1985). Two receptor systems for corticosterone in rat brain: microdistribution and differential occupation. *Endocrinology*, 117(6):2505–2511.

Sadasivam, M., Ramatchandirin, B., Balakrishnan, S., and Prahalathan, C. (2015). Tnf-α-mediated suppression of leydig cell steroidogenesis involves dax-1. *Inflammation Research*, 64(7):549–556.

Shen, W.-J., Patel, S., Natu, V., Hong, R., Wang, J., Azhar, S., and Kraemer, F. B. (2003). Interaction of hormone-sensitive lipase with steroidogeneic acute regulatory protein facilitation of cholesterol transfer in adrenal. *Journal of Biological Chemistry*, 278(44):43870–43876.

Song, K.-H., Park, Y.-Y., Park, K. C., Hong, C. Y., Park, J. H., Shong, M., Lee, K., and Choi, H.-S. (2004). The atypical orphan nuclear receptor dax-1 interacts with orphan nuclear receptor nur77 and represses its transactivation. *Molecular Endocrinology*, 18(8):1929–1940.

Spiga, F. and Lightman, S. L. (2015). Dynamics of adrenal glucocorticoid steroidogenesis in health and disease. *Molecular and cellular endocrinology*, 408:227–234.

Spiga, F., Liu, Y., Aguilera, G., and Lightman, S. L. (2011a). Temporal effect of adrenocorticotrophic hormone on adrenal glucocorticoid steroidogenesis: involvement of the transducer of regulated cyclic amp-response element-binding protein activity. *J Neuroendocrinol*, 23(2):136–42.

Spiga, F., Waite, E. J., Liu, Y., Kershaw, Y. M., Aguilera, G., and Lightman, S. L. (2011b). Acth-dependent ultradian rhythm of corticosterone secretion. *Endocrinology*, 152(4):1448–57.

Spiga, F., Walker, J. J., Gupta, R., Terry, J. R., and Lightman, S. L. (2015). 60 years of neuroendocrinology: Glucocorticoid dynamics: insights from mathematical, experimental and clinical studies. *Journal of Endocrinology*, 226(2):T55–T66.

Spiga, F., Walker, J. J., Terry, J. R., and Lightman, S. L. (2014). Hpa axis-rhythms. *Compr Physiol*, 4(3):1273–98.

Sugawara, T., Kiriakidou, M., McAllister, J. M., Holt, J. A., Arakane, F., and Strauss, J. F. (1997a). Regulation of expression of the steroidogenic acute regulatory protein (star) gene: a central role for steroidogenic factor 1. *Steroids*, 62(1):5–9.

Sugawara, T., Kiriakidou, M., McAllister, J. M., Kallen, C. B., and Strauss, J. F. (1997b). Multiple steroidogenic factor 1 binding elements in the human steroidogenic acute regulatory protein gene 5'-flanking region are required for maximal promoter activity and cyclic amp responsiveness. *Biochemistry*, 36(23):7249–7255.

Swinburne, I. A. and Silver, P. A. (2008). Intron delays and transcriptional timing during development. *Developmental cell*, 14(3):324–330.

Tkachenko, I. V., Jääskeläinen, T., Jääskeläinen, J., Palvimo, J. J., and Voutilainen, R. (2011). Interleukins 1α and 1β as regulators of steroidogenesis in human nci-h295r adrenocortical cells. *Steroids*, 76(10):1103–1115.

Veitia, R. A. (2002). Exploring the etiology of haploinsufficiency. *Bioessays*, 24(2):175–184.

Waite, E. J., McKenna, M., Kershaw, Y., Walker, J. J., Cho, K., Piggins, H. D., and Lightman, S. L. (2012). Ultradian corticosterone secretion is maintained in the absence of circadian cues. *European Journal of Neuroscience*, 36(8):3142–3150.

Walker, J. J., Terry, J. R., and Lightman, S. L. (2010). Origin of ultradian pulsatility in the hypothalamic-pituitary-adrenal axis. *Proc Biol Sci*, 277(1688):1627–33.

Watt, M. J., Holmes, A. G., Pinnamaneni, S. K., Garnham, A. P., Steinberg, G. R., Kemp, B. E., and Febbraio, M. A. (2006). Regulation of hsl serine phosphorylation in skeletal muscle and adipose tissue. *American Journal of Physiology-Endocrinology and Metabolism*, 290(3):E500–E508.

Windle, R., Wood, S., Shanks, N., Lightman, S., and Ingram, C. (1998). Ultradian rhythm of basal corticosterone release in the female rat: Dynamic interaction with the response to acute stress 1. *Endocrinology*, 139(2):443–450.

Winnay, J. N. and Hammer, G. D. (2006). Adrenocorticotropic hormone-mediated signaling cascades coordinate a cyclic pattern of steroidogenic factor 1-dependent transcriptional activation. *Mol Endocrinol*, 20(1):147–66.

Xu, B., Yang, W. H., Gerin, I., Hu, C. D., Hammer, G. D., and Koenig, R. J. (2009). Dax-1 and steroid receptor rna activator (sra) function as transcriptional coactivators for steroidogenic factor 1 in steroidogenesis. *Mol Cell Biol*, 29(7):1719–34.

Zhao, D., Duan, H., Kim, Y. C., and Jefcoate, C. R. (2005). Rodent star mrna is substantially regulated by control of mrna stability through sites in the 3'-untranslated region and through coupling to ongoing transcription. *J Steroid Biochem Mol Biol*, 96(2):155–73.

Æsøy, R., Mellgren, G., Morohashi, K.-I., and Lund, J. (2002). Activation of camp-dependent protein kinase increases the protein level of steroidogenic factor-1. *Endocrinology*, 143(1):295–303.